2015

Enhanced Structure and Crystallinity of Semiconducting Polymer Films Through Electrospray Deposition

Johan Rodriguez
University of Central Florida

ENHANCED STRUCTURE AND CRYSTALLINITY OF SEMICONDUCTING POLYMER FILMS THROUGH ELECTROSPRAY DEPOSITION

by

JOHAN RODRIGUEZ
B.S. University of Central Florida, 2012

A thesis submitted in partial fulfilment of the requirements
for the degree of Master of Science
in the Department of Mechanical and Aerospace Engineering
in the College of Engineering and Computer Science
at the University of Central Florida
Orlando, Florida

Summer Term
2015

Major Professor: Weiwei Deng

ABSTRACT

Electrospray atomization is a method that uses electrical stresses as the means of generating charged droplets. The fundamental working principles of electrospray have previously been extensively studied and demonstrated to have monodisperse droplet size distribution, good stability and scalability. Electrospray is a bottom-up deposition method which opens up the possibility of a roll-to-roll compatible process and is functional at regular atmospheric conditions. Due to this set of positive qualities, this atomization method holds promise as a means of solution based material processing that is cost effective and scalable. Conjugated polymers are among the solution processable materials of most interest, poly(3-hexylthiophene)(P3HT) standing out as one of the most extensively studied. Applications of P3HT as a p-type semiconductor have been demonstrated in devices like organic solar cells, light emitting diodes and transistors. Improvements in the performance of the mentioned devices have been correlated with a higher degree of crystallinity as well as the film structure in the case of organic solar cells.

The effects of different electrospray process parameters are investigated and various P3HT film structures are presented in this study. Electric repulsion present within the droplets in electrospray and evaporation of the solvent were used to obtain high aspect ratio features on the P3HT films. A clever design for the electrospray nozzle devised to improve the process stability is presented. Also, the crystallinity of the films was characterized using grazing incidence x-ray diffraction (GIXRD) and ultraviolet visible spectroscopy. All results in this study are presented as a comparison to spin coated control process. The GIXRD results suggest that the electrospray process produces crystallites that have an orientation opposite of the orientation observed in the spin coated process. Analysis of the ultraviolet visible spectroscopy absorption spectrum shows a red-shift, signaling an increase in the crystallinity. Lastly, good contact between the deposited P3HT and the substrate was confirmed using conductive atomic force microscopy (CAFM).

To my mother, the most influential person in my life and whose unconditional support has been essential in all that I do.

ACKNOWLEDGMENTS

I would like to thank Weiwei Deng and Danvers Johnston for their invaluable advisement and help throughout this study.

TABLE OF CONTENTS

LIST OF FIGURES

LIST OF TABLES

CHAPTER 1: INTRODUCTION AND BACKGROUND

Electrospray atomizers have drawn attention due to numerous characteristics that make it a promising method of deposition for solution based processing of materials. The droplet size and the uniformity are important due to their influence in the scale of the application and the uniformity. Keqi Tang and Alessandro Gomez determined the droplets typically break up into two groups, the primary droplets and the satellite droplets that are in diameter roughly one third the size. Among the primary droplets, which compose roughly 97% of the volume and 85% of the charge, the size distribution is considered monodisperse. In addition to the monodispersity, droplets diameters ranging from a few nanometers to tens of micrometers can be achieved[43][9]. The electrical charges also present qualities useful for solution processing such as self dispersion and control over the path of the droplets. Setting up an electrospray deposition system is relatively simple with the main components being a needle, high voltage power supplies and a pump. Overall, the promise of electrospray deposition relies on the simple operation and droplet characteristics. The great potential of electrospray deposition of polymers was demonstrated by making spherical polymer particles ranging form 600 nm to 2 μm[4]

P3HT forms part of a group of polymers referred to as conjugated polymers. More specifically, P3HT is a monomer consisting of a thiphene ring and a alkyl side chain as illustrated in figure 1.1. Conjugated polymers are semiconductors, stable in solution, and can also be photoactive. These characteristics have led to applications common with other semiconductor material devices like organic solar cells [48][13], light emitting diodes [39][36] and transistors [29]. In these devices, P3HT is implemented as a p-type electron donor material and typically coupled with Phenyl-C61-butyric acid methyl ester (pcbm) as the n-type semiconductor. In organic solar cell devices the P3HT and the PCBM are deposited through spin coating as a blend resulting in a disordered heterojunction. However, spin coating is uncapable of delivering an the optimized ordered heterojunc-

tion necessary to increase the efficiency [13]. Other methods of processing conjugated polymers through inkjet printing [7] and screen printing [37].

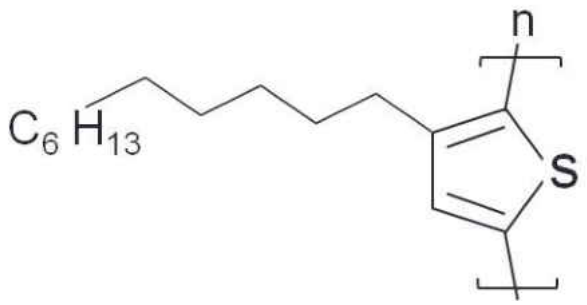

Figure 1.1: Schematic of chemical structure of P3HT.

The Distinct Properties of Electrospray

For close to a century electrospray has been extensively studied since John Zeleny first explained and photographed the effects of of applying an electric field onto a liquid meniscus [49] [50]. Before John Zeleny, more fundamental studies of the behavior of liquid jet breakup and effects of electric charges on liquid droplets were conducted by Lord Rayleigh[35][34]. The electric field at which the liquid meniscus is exposed to electrospray affects the shape of the meniscus. These different meniscus shapes have been identified and are referred to as modes [49] [50][12]. In the absence of an electric field, the meniscus will only drip at the low flow rates in which electrospray works. As the electric field is gradually increased the dripping becomes faster until the meniscus goes into pulsing mode, cone-jet mode and multi-jet mode sequentially. In the pulsing mode, the meniscus appears as a blurred cone while in cone-jet mode it appears as a well defined sharp image of a cone and the multi-jet appears as multiple jets ejecting from the meniscus. Note, that these are not the only modes identified in electrospray but only the ones observed in this study. Of most

interest is the cone-jet mode, also referred to as Taylor cone, in which the coulombic repulsion and the surface tension are in balance and form a meniscus in the shape of a cone as shown in figure 1.2(a). In the apex of the cone, a jet emerges which breaks up into charged droplets downstream. Figure 1.2 also shows the jet(a) and the resulting spray profile after the jet breaks up (b).

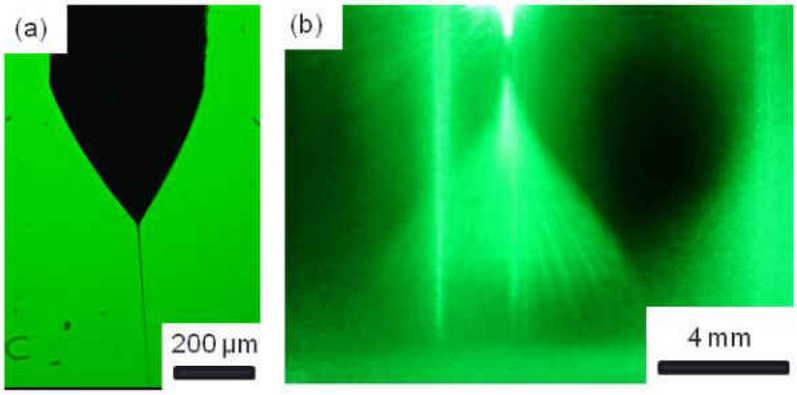

Figure 1.2: (a) Meniscus and (b) profile of electrospray in cone-jet mode.

The electric charges on the droplets distinguishes electrospray from other forms of atomization. First, the repulsion between the droplets causes the spray to self disperse and prevent droplet to droplet agglomeration. Also, the path of the droplets from the jet to the collecting substrate could possibly be controlled by use of external electric fields as it is done in quadrupole mass spectroscopy. Control over the breakup of an electrospray jet using a lateral alternating electric fields has already been demonstrated [47]. The material utilization efficiency is superior in electrospray solution base processing since the charged droplets are guided onto the collecting substrate to discharge. The degree to which the spray profile opens or closes can also be controlled by increasing or decreasing the electric field. However, this is limited since the cone-jet mode will only remain stable between a small range of voltages. The range of the electric field acting on the droplets can be extended by adding an intermediate electrode, termed as an extractor, to isolate the electric field near the meniscus[18][4]. Apart from the external effects of the electric charges, the droplets

are also subject to coulombic repulsion of the charges within. This has been theoretically[35] and experimentally[23] studied and demonstrated to lead to instabilities in the droplets. Also, the presence of electrical charges on a droplet has been demonstrated to improve the wetting as the droplets impact an electrically conducting surface[17].

The balance of the coulombic repulsion and surface tension necessary to maintain a cone-jet outlines the importance of the conductivity of the liquid K and the surface tension γ as the two liquid properties that play the most important role. Besides the stability, it is also of interest to know which properties and parameters affect the droplet size of the spray. Equation 1.1 is a scaling law for the diameter of the droplets d obtained theoretically and confirmed experimentally for electrospray in the cone-jet mode of various solvents[24].

$$d \sim \left(\frac{\rho \varepsilon_o Q^3}{\gamma K} \right)^{1/6} \tag{1.1}$$

The flow rate is denoted by Q, the density of the solvent by ρ and ε_o the permittivity of the medium. Note that for a particular solution and a medium, the only parameter that can be varied is the flow rate. Also, the droplet size is independent of the the nozzle diameter and viscosity of the liquid that is being electrospray. Although equation 1.1 is very useful to gain a sense of the effects of changing the flow rate or the fluid properties mentioned, caution should be exercised when using the equation to get definite values for the droplet diameter. It should be noted that equation 1.1 is the result of a string of studies to determine the scaling laws of electrospray [15] [22] [8].

The biggest concern impeading the wide implementation of electrospray deposition on an industrial scale is the low flow rates of operation for a single emitter. Efforts to increase the throughput by increasing the amount of emitters, termed multiplex electrospray, have proven successful[30] [18] [32] [19]. This scale up method is attractive since the flow rate per nozzle and by association the droplet size are maintained constant as the total flow rate is scaled up. Also, the size of the

multiplex emitters has been demonstrated to be very compact with the density of emitters being an outstanding $11,547\ sources/cm^2$ [19]. Models for multiplex electrospray have been developed along with design guidelines [47][16].

The Anisotropic properties of P3HT

P3HT has a tendency to aggregate into crystals as the concentration increases when the solvent is evaporated [28][11]. These crystals become buried in a matrix of amorphous P3HT forming a semi crystalline solid and have a tendency to align in the edge-on orientation when spin coated [29]. Figure 1.3 demonstrates a P3HT crystal in different orientations and depicts the different directions with the notation in accordance with previous studies [26][2][25][38]. Note, in figure 1.3, that the lamellar lattice across the alkyl chain and the $\pi - \pi$ stacking lattice alternate directions from face-on to edge-on alignment. Due to the significant difference in the different direction of the P3HT crystals, the electrical properties become anisotropic. It has been determined that charge mobility along the alkyl chains is roughly 3 orders of magnitude lower than along the conjugated backbone and the $\pi - \pi$ stacking [38]. Hence, referring to figure 1.3, in the face-on orientation the mobility is higher normal to the plane and in edge-on orientation the mobility is higher along the plane. Also, the charge mobility has been demonstrated to increase as the conjugation length increases [6]. In order to improve the in-plane mobility for edge-one oriented devices, efforts to increase the cojugation length have been effective. Studies have successfully demonstrated an increase in the conjugation length through thermally annealing samples [10][45][20][28] by processing with high boiling point solvents [11]. Other studies have demonstrated control over the orientation of the P3HT crystals by using grids to induce face-on orientation of the crystals[26][2][25].

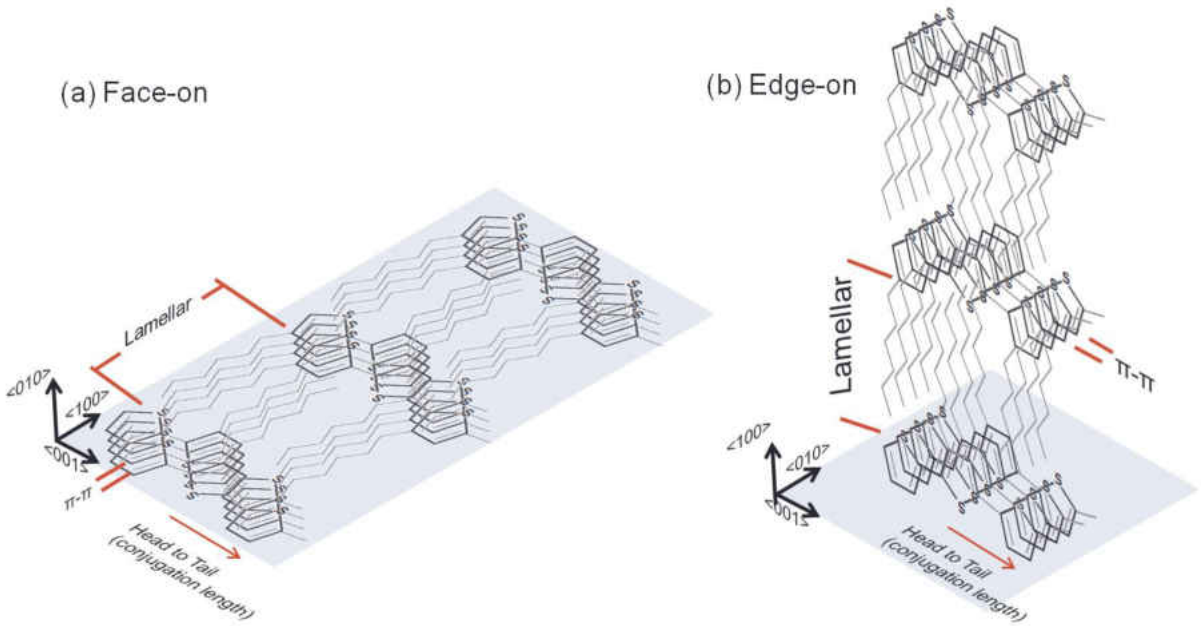

Figure 1.3: Schematics of P3HT crystals in (a)face-one orientation and (b)edge-on orientation with lamellar, $\pi - \pi$ latices and head to tail (conjugation length) direction along polymer backbone.

CHAPTER 2: METHODOLOGY

Figure 2.1 outlines the experimental setup with all the components, typical parameters and axis of motion. The nozzle was directly connected to a $100\mu L$ glass Hamilton syringe and then to a Chemyx nanojet syringe pump. With this size of the syringe, the resolution of the syringe pump is about 0.5 nL. The nozzles used in this study were a $100\mu m$ outer diameter needle and a 27 gauge needle with a $410\mu m$ outer diameter. A small sheet heater was wrapped around the glass syringe to maintain a temperature of roughly 60^oC. The syringe pump was fixed onto a 1D hand turned motion stage to control the distance between the area where the spray is initiated and the collecting substrate. White or green LED lights were used as back-light to obtain a shadow graph image using a Cannon Rebel EOS camera with an attached and extended 10X magnification lens. The camera was attached to a 3D Newport hand turned motion stage to position and focus the camera field of view onto the nozzle tip. The high potential end of an Acopian (model P020HP1. 5M) high voltage power supply was clipped to the nozzle while the ground was connected to the collecting substrate. The substrate was attached to a Newport TS series liner motion stage. The motion stage was controlled using a software package called EMC that allows programming of linear velocity, acceleration and quantity of coatings.

Separate solutions were prepared using 1 wt% and 0.1 wt% P3HT in Chorobenzene. The solution was filtered using at PTFE $0.22\mu m$ pore filter to eliminate undissolved P3HT aggregates. Triflouroacetic acid and acetone were added by 1 % and 10 % by volume respectively in order to enhance the electrical properties of the solution. The P3HT solution then had to be maintained at 60^oC to maintain a stable solution without P3HT aggregation. The concentration of P3HT was changed in order to change the size of the resulting P3HT films. A silicon wafer coated with a 300 nm copper film was used as the base to collect the P3HT particles and films. The copper coated wafers were cleaned through a process that started dipping cleaved pieces of roughly $3x3cm$ into

acetone, ethanol and DI water bath sequentially and allowing at least 30 minutes in each step. A film of (poly(3,4-ethylenedioxythiophene) polystyrene sulfonate) PEDOT:PSS was then spin coated onto the silicon wafers using a angular velocity of 2000 rpm for 45 seconds preceded by 500 rpm for 5 seconds resulting in a coating of about $50nm$. The purpose of the PEDOT:PSS coating was to generalize the surface effects on all the samples. The water based PEDOT:PSS solution was prepared for spin coating by first filtering the solution using a PES $0.22\mu m$ pore filter and then adding Isopropanol alcohol in equal parts by volume to the filtered solution. The Isopropanol alcohol was introduced to decrease the surface tension of the PEDOT:PSS solution and allow for better coverage of the silicon wafer.

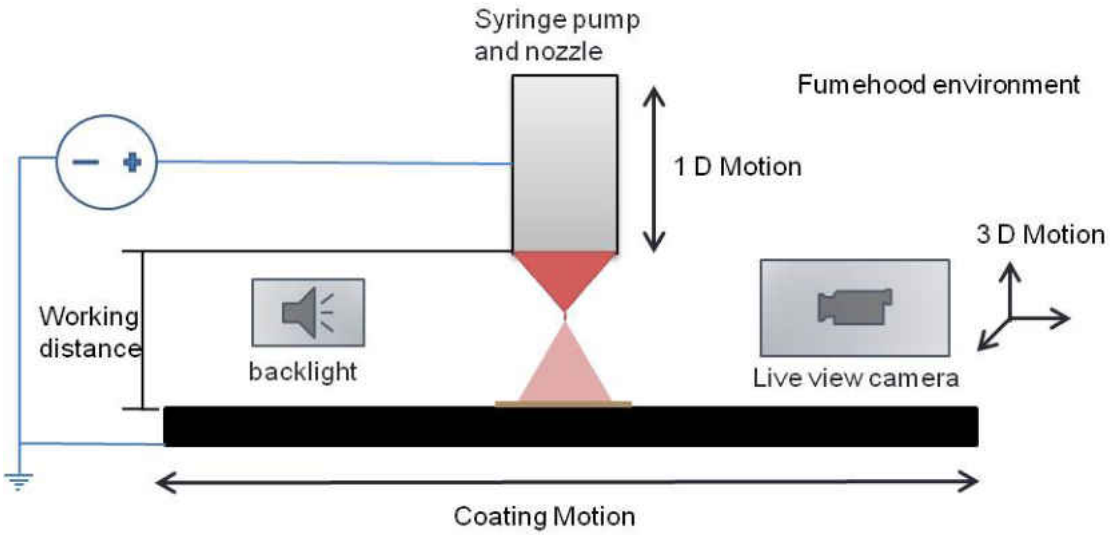

Figure 2.1: Experimental setup

Characterization Methodology

The GIXRD measurements were carried out at the National Synchrotron light source at Brookhaven National Laboratory. The scattered x-rays were collected in a 2D detector. The profile cuts across the peaks presented in figures 4.6 and 4.7 were taken using Gwiddion software package. ImageJ software was used for the polar profile cuts presented in figures 4.4 and 4.5. To measure the optical transmission/absorbance spetrum of the films between 200 and 800 nm a Cary Win UV spectrometer was utilized to obtain the transmission/absorbance spectrum of the samples between 200 and 800 nm. Both films were deposited on glass coated with fluorine doped tin oxide (FTO) and PEDOT:PSS with the same conditions detailed in section 3.2 substrate preparation. An additional film of only FTO coated glass coated with PEDOT:PSS was prepared to subtract the background signal from the absorbance measurement. The AFM used was a Veeco Manifold multimode model along with a Conductive AFM module. The module consisted of a voltage actuator, a signal amplifier and a current sensor. In order to use the CAFM module, the AFM was set in contact mode at constant deflection and tip was an Olympus platinum coated silicon tip with a $28 \pm 10nm$ diameter. In this mode, this tool can reach spatial resolutions in the atomic scale. The samples for this measurement needed an extra process which is detailed in Atomic Force Microscopy section of the characterization chapter. Gwiddion was also used to plot the space and electrical current data. A Zeiss ULTRA-55 FEG Scanning Electron Mircroscope (SEM) was used in all the SEM images presented in this study.

CHAPTER 3: PROCESS DEVELOPMENT

Cone-jet Stabilization

Electrospray of pure solvents like ethanol is relatively simple to achieve and remains stable for long periods of time. However, the process becomes many times more difficult when electrospraying solutions of dissolved material or suspensions. The solid content in the solutions can give rise to problems such as clogging or solidification of the cone-jet. The latter issue was present in electrospraying of the P3HT solution as it is presented in figure 3.1(b). The initial state of the electrospray was as demonstrated by figure 3.1 (a) but after some time, typically between 1 to 5 minutes, the cone-jet would evolved to that presented in figure 3.1(b). A hard shell of P3HT built up in the cone-jet which prevented the smooth flow of the solution. This shell had negative effects on the spraying process such as tilting the jet to the side as can be observed in the photograph. Also, as the shell became bigger it eventually stopped the flow or would break off and disturb the process. Furthermore, the build up of this shell consumed P3HT and therefore made it difficult to know the actual flow rate of the P3HT material.

It was initially contemplated that the formation of the shell was caused by rapid drying in the conejet. Therefore it was of interest to reduce the evaporation rate of the solvent caused on the cone-jet by its near environment. As dictated by Fick's first law, equation 3.1, the diffusion flux J is calculated by the negative product of the diffusion coefficient D and the concentration gradient $\nabla\phi$. For the case of electrospray of the polymer solution, the diffusion flux corresponds to the evaporation rate and the concentration gradient of interest is that of the chlorobenzene solvent.

$$J = -D\nabla\phi \tag{3.1}$$

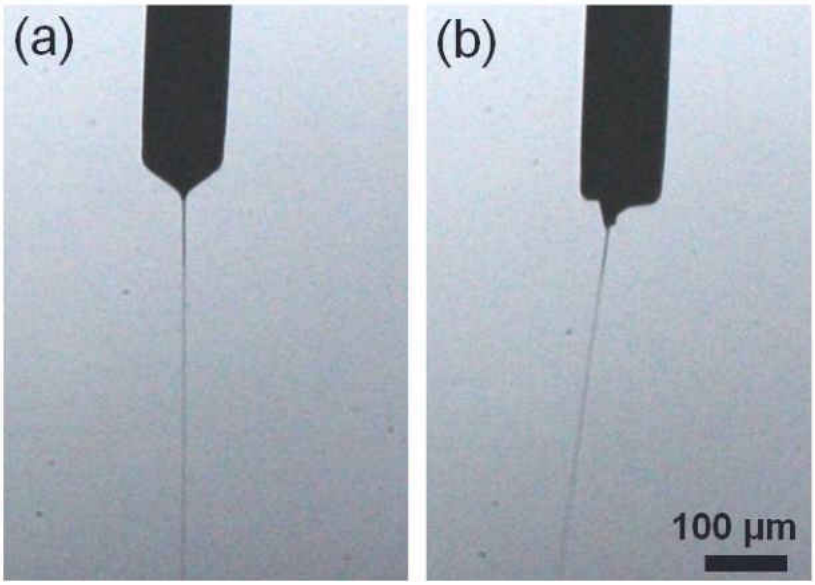

Figure 3.1: (a) Initial state of electrospray using regualar $100\mu m$ outer diameter nozzle and (b) build up of P3HT in the cone-jet after short time.

Then, by equation 3.1, the evaporation rate can be lowered by decreasing the concentration gradient of chlorobenzene. To achieve this task, the experiment setup illustrated in figure 3.2 was constructed. This experiment setup is a modification of the setup presented in figure 2.1. The electrospray was enclosed within a acrylic cylindrical chamber to ensure that the chlorobenzene vapor did not escape the near environment. Also, an intermediate electrode with a slit in the bottom was introduced to further enclose the near environment. On the top, the chamber was enclosed with parafilm. A small hole was made on one side to allow for the visualization of the electrospray. A heated vial filled with liquid chlorobenze was introduced inside of the chamber to ensure that a large concentration of the solvent. It is likely that the chamber also affected the diffusion coefficient D, but the effects are to lower the evaporation rate since it would eliminate any force convection caused by the flow of the fumehood. After running the electrospray multiple times inside of the chamber filled with chlorobenzene, the effects observed in figure 3.1 (b) still persisted. Since no

substantial difference was noticed, it was determined that the solvent evaporation in the chamber was not the cause for the P3HT aggregation shell in the cone-jet.

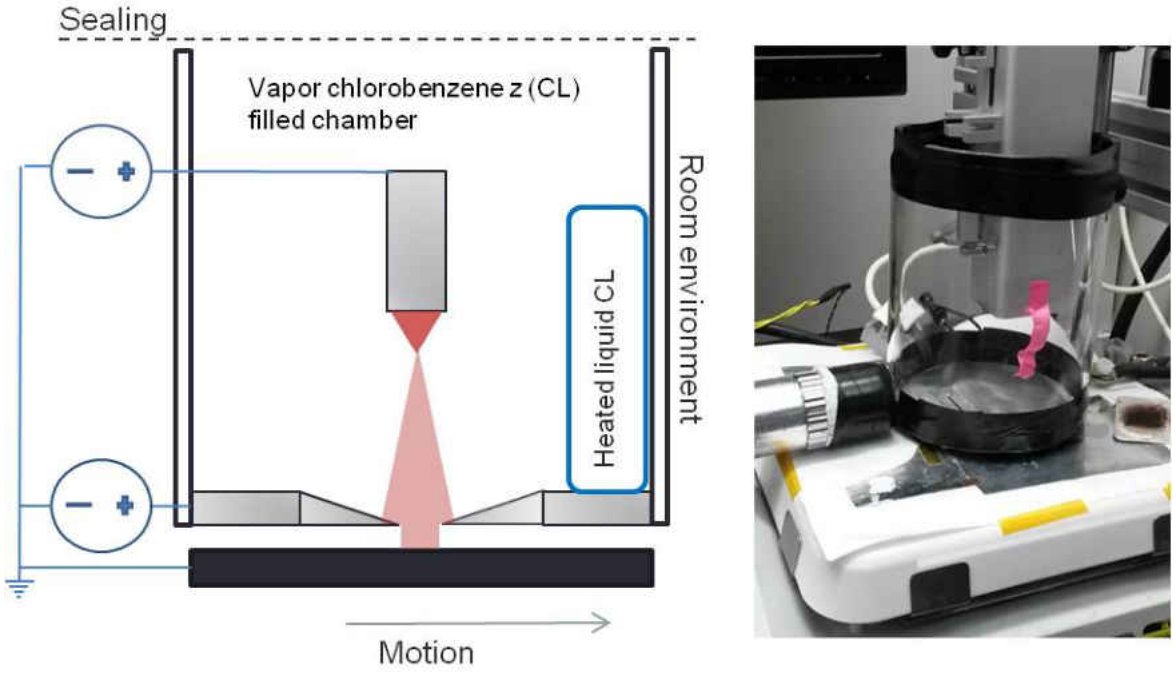

Figure 3.2: Schematic and photograph of modified experimental setup including chlorobenzene filled chamber.

Studies have demonstrated experimentally[31] and through numerical simulation[27] that the stability of an electrospray in cone-jet mode can be improved by inserting a tip concentric with the nozzle. The tip prevents the creation of recirculation cells that are present in cone-jet mode by forcing the flow along the drillbit channels and the surface. In the case of the P3HT solution, the recirculation cells allowed the solution to remain at temperatures below the temperature for which the solution was stable. After some time, the P3HT present in the recirculation cells would drop out of solutions and form the aggregations observed in figure 3.1 (a). To imitate the concentric tip design, a drillbit of roughly $200\mu m$ was inserted in to 27 gauge needle as shown in figure 3.3. The drill bit was a simple and effective solution since it was easy to align concentrically and provided

channels for the flow. The drillbit was inserted into the needle by using tweezers to hold the needle and the drillbit, a microscope to visualize and pliers to slightly deform the needle to press the drillbit in place. Figure 3.3 (b) demonstrates the electrospray using the nozzle with concentric drillbit which remained stable for as long as the process required.

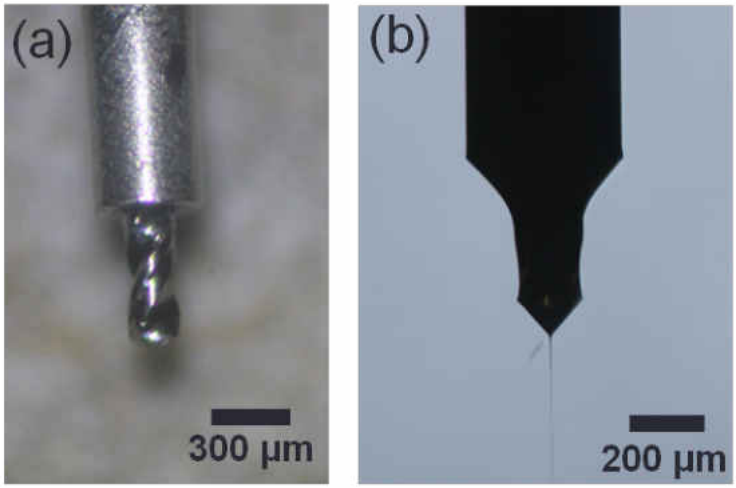

Figure 3.3: (a) Modified nozzle with concentric drillbit and (b) electrospray in stable cone-jet mode using drillbit nozzle

Morphology of P3HT Films

Electrospray distinguishes itself from other atomizers in that the droplets are electrically charged when they break apart from the jet. This introduces electric repulsion between the droplets as well as within the particular droplets. The effects of repulsion within the droplet have been theoretically studied by Lord Rayleigh where he determined that a droplet of diameter d can only contain a finite amount of charge q before developing an instability. The instability develops as a result of the electrical repulsion force overpowering the binding surface tension force in the liquid gas interface of the droplet. Figure 3.4 illustrates a free body diagram of the surface of a droplet under the

influence of surface charges. The charge quantity q is termed the Rayleigh limit and is dictated by equation 3.2 where γ is the surface tension of the liquid of the droplet and ϵ_o is the permittivity of the medium, air in this case.

$$q^2 = 8\pi^2 \epsilon_o \gamma d^3 \tag{3.2}$$

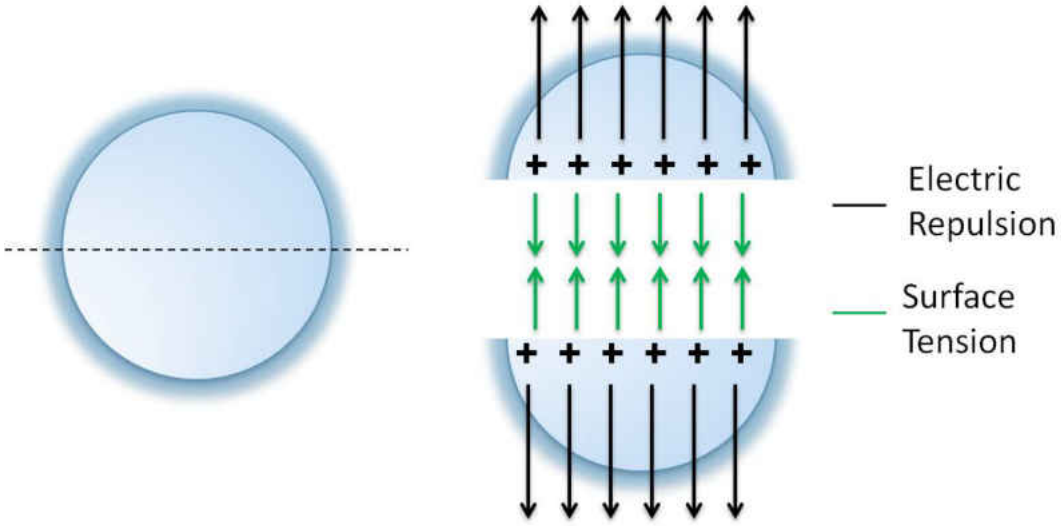

Figure 3.4: In the left, droplet suspended in space where dashed line represents the cutaway section used in the free body diagram on the surface of a charged droplet represented in right.

The effects of electrical charges within a droplet have also been studied experimentally [23]. Alessandro Gomez and Keqi Tang determined that the instability happens when the charge of the droplets is between 70% to 80% of the Rayleigh limit. The instability was visualized in a process termed coulombic fission where a jet forms on the surface of the droplets and begins to eject smaller droplets. In the case of electrospray, coulombic fission is approach as a result of evaporation. As the droplet losses its mass the its diameter decreases exponentially but the charge on the droplet remains constant. The decrease in diameter affects the right hand side of equation 3.2 and as that value approaches 70 % to 80% of the left hand side, coulombic fission will occur.

The previously mentioned study by Gomez and Tang only considered the effects of electric charges within a droplet composed of a single liquid with no solid content. The effects of coulombic fission in droplets composed of poly(lactic-co-glycolic acid) (PLGA) solution have been demonstrated to show unusual morphologies in the particles resulting after full drying[3]. The cause for the unusual morphologies was the interactions between the individual PLGA chains creating a network, termed polymer entanglement, and maintaining the droplets shape as the droplet approached coulombic fission. Figure 3.5 explains the results by comparing the situation of a charged droplet of pure solvent and one that contains polymer dissolved within it. As the solvent in the droplet evaporates causing it to approach the Rayleigh limit, the polymers entangle and maintain the droplet structure instead of splitting into multiple droplets. Contrarily, charged droplets generated through electrospray of polymer solutions that do not reach coulombic fission have been shown to result in spherical shapes and circular blobs [4] [5] [42] [33] [51]. The main parameters associated with the resulting morphologies are the flow rate of the process and the polymer concentration in the solution [3].

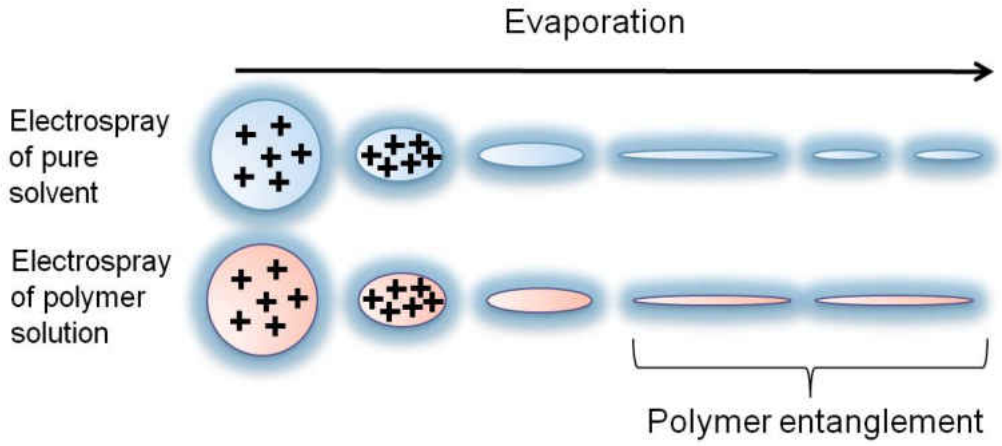

Figure 3.5: Comparison of pure solvent vs polymer solution charged droplet undergoing evaporation

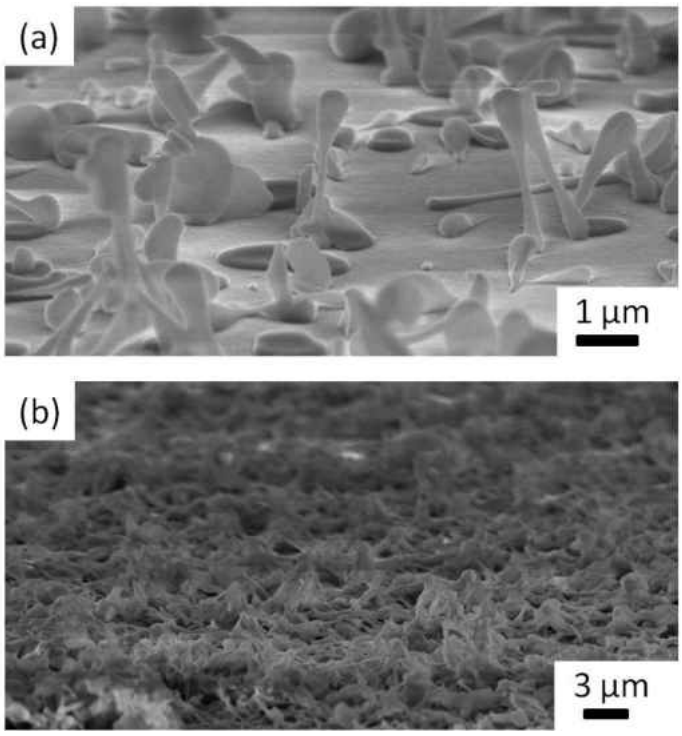

Figure 3.6: 1 wt % P3HT, 100 $\frac{\mu L}{hr}$, sample SEM image taken with 70^o angle perspective. (a) Low coating density sample and (b) high coating density sample.

The phenomena illustrated in figure 3.5 applied to electrospray deposition of P3HT is presented in figure 3.6. High aspect ratio pillar like features can be observed in the SEM image in figure 3.6 (a). The cause for the features observed in the image is attributed to coulombic fission as the solvent evaporates. Although the morphology is not exactly consistent with those presented in the study with PLGA solutions [3] the coulombic diffusion is still likely the cause of the elongation of the features. These pillar like features, in figure 3.6, are roughly 3 μm in length, 500 nm in width near the two extremes and 150 nm width in the center. This constitutes to an aspect ratio ranging from roughly 6 in the extremes to 20 using the center width. Apart from the more notable high aspect ratio pillars, there also appear to be some features that broke apart in the middle where the pillars are the thinnest. These appear as rounded top cone like structures and are scattered

throughout. Also, there are droplets that landed in liquid state present as disk like blobs laying flat in the substrate. Another remarkable characteristic of the electrospray samples is the affinity of the pillars to land vertically. Although we cannot claim that all particles are vertical, the majority of the pillars are in the upright position. An easily observable exception is the particle near the middle of the image in the top right quadrant. In figure 3.6 (b), a sample of the same electrospray conditions is presented but with a higher quantity of P3HT. This was achieved through a higher quantity of coatings at the same velocity. The features are no longer distinguishable due to the high density of the P3HT. The sample in figure 3.6 (b) is a testament to the stability of the electrospray through the coating process. Note that the images were taken with a 70^o perspective and to more accurately estimate vertical distances, the measurements must be divided by $\sin(70^o)$.

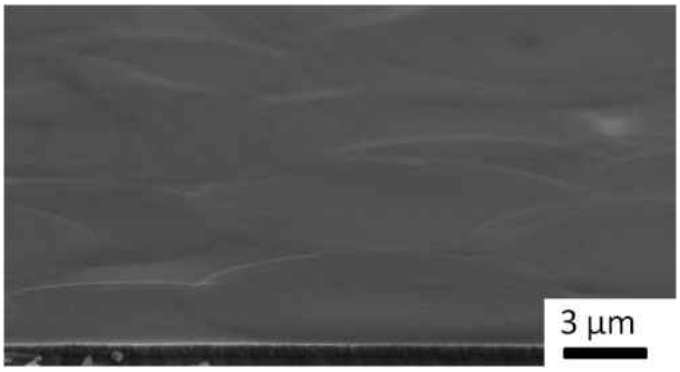

Figure 3.7: 1 wt % P3HT, 400 $\frac{\mu L}{hr}$, sample SEM image taken with 70^o angle perspective

The ability to fabricate semi-smooth continuous films of P3HT using electrospray deposition is evident by observing figure 3.7. This sample was fabricated at a volumetric flowrate that was 4 times greater than the samples presented in figure 3.6 leading to larger droplets. Due to the higher quantity of solvent present in these droplets, the drying time is not sufficient to remove all of the solvent. This leads to the droplets landing in the liquid phase and free to deform, resulting in thin disk features with a diameter roughly 14 μm. Note that the SEM image was taken at a 70^o angle

perspective which gives the impression that the features are oval like.

As previously stated, the concentration of the polymer in the solution is one of two main parameters that affects the morphologies. The sample presented in figure 3.8 was processed with a polymer concentration that was 10 times less than the sample presented in figure 3.6. As expected, the decrease in concentration results in features that are smaller in size. The height of the features is roughly 150 nm and the width 200 nm. Note that in height, the pillar like features in figure 3.6 are larger than the features in figure 3.8 but the widths are of comparable size. The cause for the non presence of high aspect ratio features is likely that the concentration of polymer in the solution was not enough to cause entanglement before coulombic fission allowing the droplets to freely break into smaller droplets.

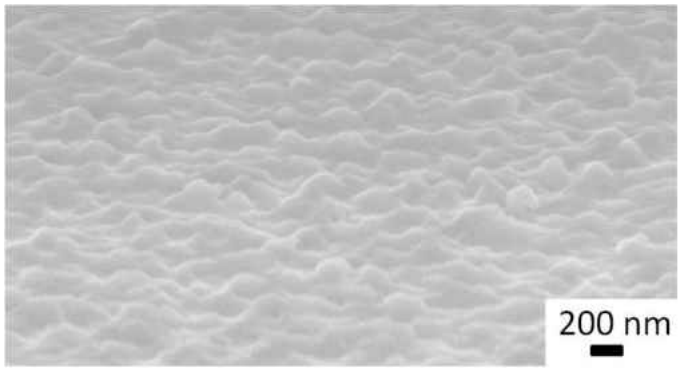

Figure 3.8: 0.1 wt% P3HT, 100 $\frac{\mu L}{hr}$, sample SEM image taken with 70^o angle perspective.

Effects of Residence Time Varied by Changing Working Distance

The working distance plays an important role in the electrospray deposition process since it is coupled with drying time. A working distance that is too short will result in droplets still in the liquid phase, due to short drying time, when reaching the substrate and proceed to deform into flat

circular disk. On the other hand, a working distance that is too long will result in dry particles reaching the substrate which will then become a collection of particles instead of a structured film. The lifetime of a droplet τ_D to completely dry is dictated by equation 3.3 where d_o is the initial droplet diameter and k is the evaporation rate [44]. Hence, if the drying time allowed by the working distance is larger than τ_D, the droplets will land dry. Conversely, if the drying time is shorter than τ_D the droplets will land wet and deform. Note, the drying time is not the only parameter that is important for the total removal of the solvent. Other parameters like diffusion constants and densities, embedded into the evaporation rate k, are also important. However, the drying time is the only parameter being varied during the experiment by changing the working distance.

$$\tau_D = \frac{d_o^2}{k} \tag{3.3}$$

It is important to determine the point at which the transition from wet to dry happens in the spray. To do so, the experiment setup presented in figure 2.1 was modified by placing the collecting substrate at an incline of 20^o angle and an intermediate electrode, presented in figure 3.9. The modified setup allowed the working distance to become variable with the lateral translation of the substrate so that as the substrate marched to the right, the working distance would gradually increase. The motion stage on which the substrate was placed was programmed to march 5 mm laterally and pause for 10 seconds in a point of collection. The 5 mm lateral increments resulted in 1.82 mm vertical increments in the working distance. In addition to the inclined substrate, an intermediate electrode was place between the nozzle and the substrate. The purpose of the intermediate electrode was to mask the circular spray profile into a thin slit so that a point of collection along the inclined substrate would not interfere with the adjacent points of collection. This effect can be observed in figure 3.9 (c) where the spray profile passing through the intermediate electrode is photographed.

The result obtained by using the modified experimental setup are presented in figure 3.10. The

SEM images presented in figure 3.10 (a,b,c) show P3HT deposition samples that are overwhelmingly composed of large circular features resulting from droplets landing wet. However, figure 3.10 (b,c) show small amounts of droplets that appear to have landed dry. The transition from mostly wet to dry seems to occur in figure 3.10 (d), corresponding to a working distance of 21.4 mm, where the majority of the particles seem to be dry. Figures 3.10 (e,f) continue to show mostly dry particles with only a few spots in (e) that seem to be the result of droplets landing wet. Aside from determining an optimal working distance, it is important to notice the stark difference between figure 3.10 (c) and (d). Although the difference in the working distance is only 1.82 mm, (c) is mostly composed of droplets that landed wet and (d) of droplets that landed mostly dried, meaning that most droplets dried in nearly the same drying time. Since the drying time is directly related to square of the diameter, equation 3.3, it can be concluded that the diameter of most droplets is nearly the same.

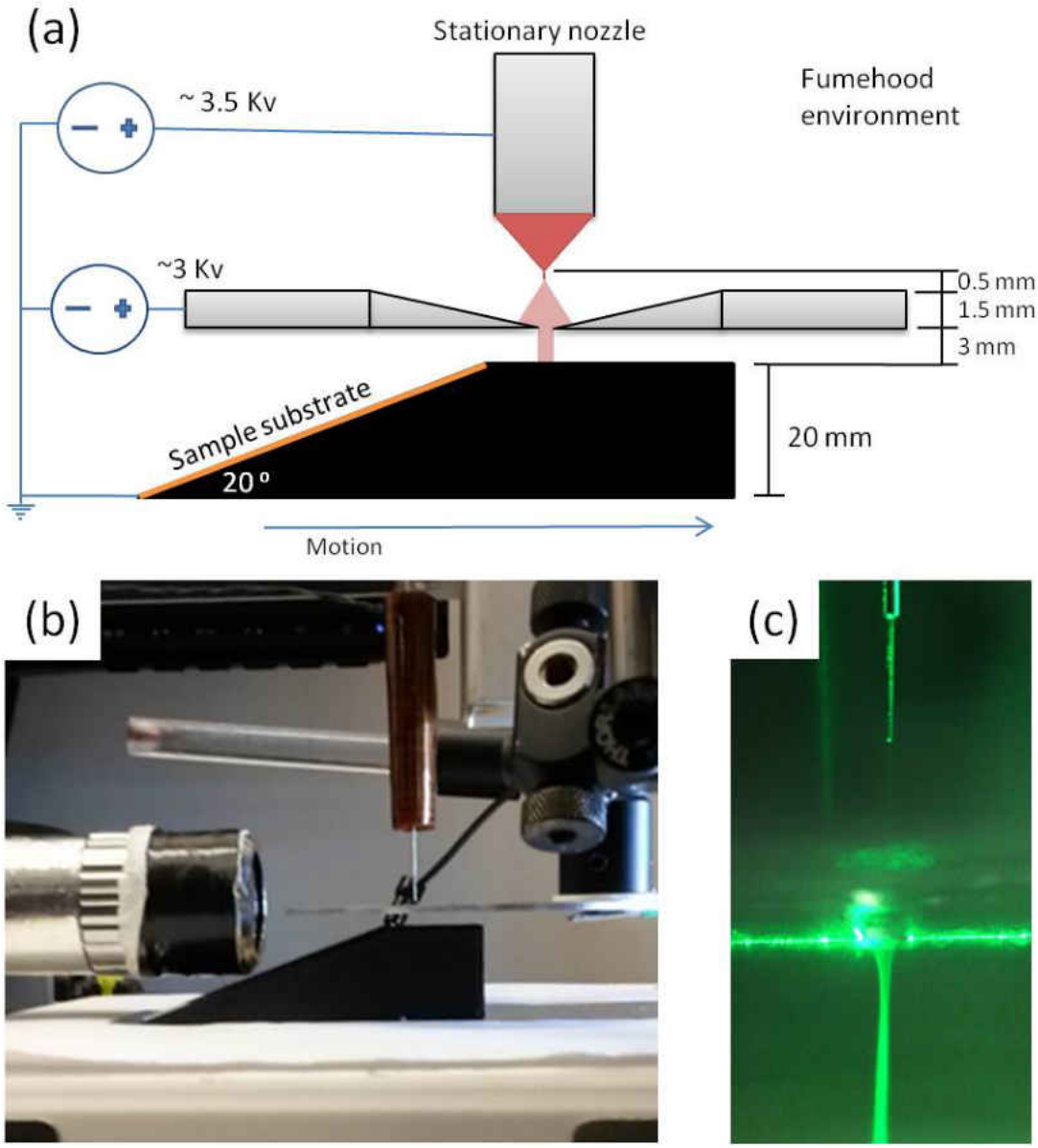

Figure 3.9: (a)Schematic of experimental setup with inclined substrate. (b) Photograph of experimental setup illustrated in (a). (c) Magnified photograph of spray profile after passing through middle electrode.

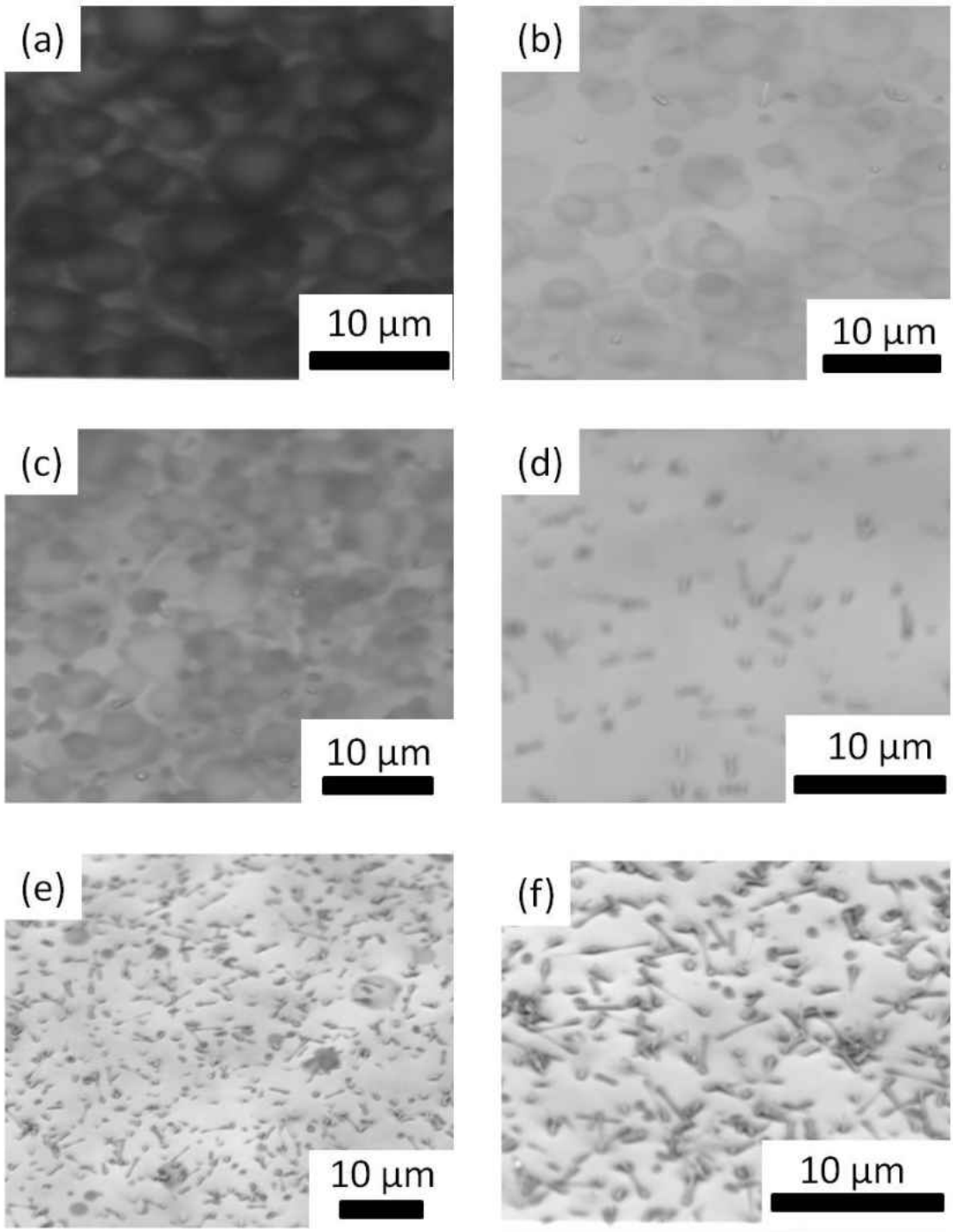

Figure 3.10: SEM images of electrospray samples collect at a working distance of (a)=15.9 mm , (b)=17.8 mm , (c)=19.6 mm , (d)=21.4 mm , (e)=23.2 and (f)=25.0 mm.

CHAPTER 4: CHARACTERIZATION RESULTS

The crystallinity of the P3HT films was characterized through grazing incidence x-ray (GIXRD) diffraction and UV-Visible spectroscopy. GIXRD is an effective tool to study the intermolecular interactions of the P3HT polymers along the lamellar and $\pi - \pi$ lattices and the crystal orientation. Additionally, UV-Visible spectroscopy can be used to study the intramolecular interactions of the P3HT monomer along the polymer backbone. Both techniques in conjunction provide a complete picture of the orientation and size of the crytallites.

Grazing Incidence X-Ray Diffraction

In the GIXRD results the diffraction peaks are dictated by the Bragg equation, equation 4.1, where n is a positive integer, λ is the wavelength of the incident wave, θ is the scattering angle, and d is expressed by equation 4.2. The values of h, k and l represent the miller indices and a is the lattice spacing. The value of d for a particular lattice spacing and orientation, will give a value of θ in accordance to Bragg's equation. That value of θ will correspond to the location of the intensity peaks in the GIXRD plots.

$$2d \sin\theta = n\lambda \tag{4.1}$$

$$d = \frac{a}{\sqrt{h^2 + k^2 + l^2}} \tag{4.2}$$

figure 4.1 shows a diagram how the x-rays are diffracted by the face on aligned P3HT crystal's latices and impact the sensor. In this orientation, the lamellar $< 100 >$ lattice diffracts with a preference onto q_x axis and the $\pi - \pi$ lattice will diffract on to the q_z axis. If the crystals have edge on orientation, the diffraction would be opposite where the lammellar and the $\pi - \pi$ lattices diffract onto the q_z and the q_x axis respectively.

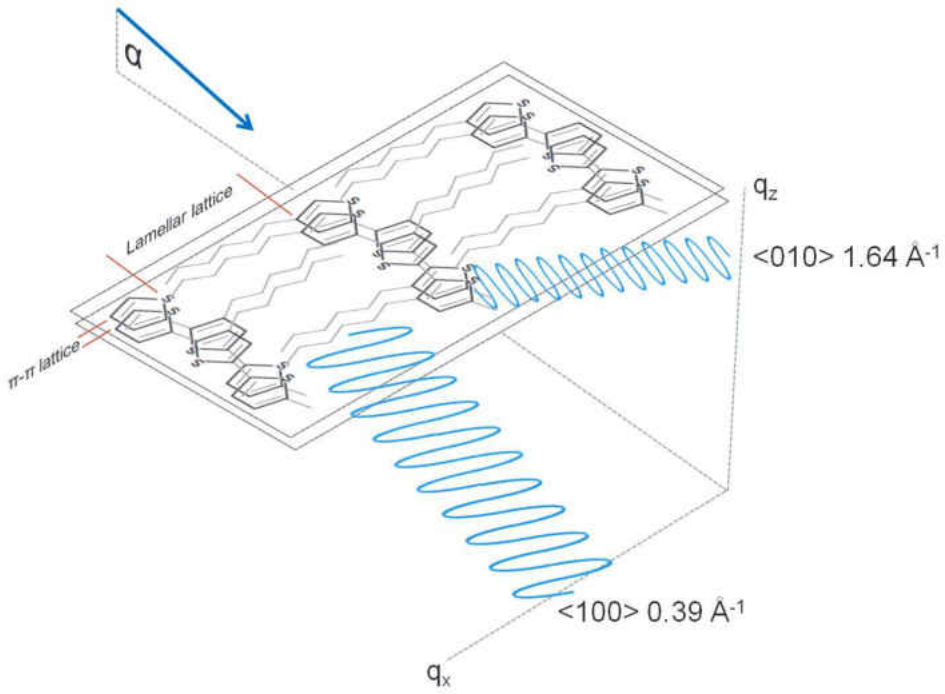

Figure 4.1: Diagram demonstrating the diffraction of X-ray beams from a face-on oriented P3HT crystal onto the 2D collector.

The 2D intensity plots produced by a GIXRD instrument illustrated in figure 4.1 can be seen in figures 4.2 and 4.3. In the case of figure 4.2, the sample is spin coated and results in a smooth thin film. It is typical for spin coated samples of P3HT to exhibit edge-on orientation which is evident in figure 4.2b where the $< 100 >, < 200 >$ and $< 300 >$ lamellar peaks are along the q_z axis and the $< 010 > \pi - \pi$ peak along the q_x axis. Note that this is the opposite situation as it is illustrated by the diagram in figure 4.1 where the P3HT crystal is shown in the face-on orientation.

The electrosprayed samples and their corresponding process conditions are denoted by table 4.1 and the SEM images as well as the GIXRD intensity plots can be seen if figure 4.3. Unlike the smooth uniform film resulting from spin coating illustrated in figure 4.2 (a), the electrospray films are mostly compose of collection elongated pillars and round features. Sample ES4 stands out the

most due to its larger features and the much higher concentration of round smooth edged disk like features. The cause of the larger features is due to the higher flowrate of sample which leads to larger droplet size. The disk like shaped particles are the droplets strike the collector partially wet and are allowed to deform due to the higher amount of solvent present in larger droplets. Of more interest are the contrast of the GIXRD intensity plots between the control spin coated sample and the electrosprayed samples. When comparing the plots in figure 4.3(b,d,f,h) to that of figure 4.2(b) there is a clear distinction of the position of the high intensity peaks corresponding to $< 100 >$ and $< 010 >$. In the spin coated sample, the $< 100 >, < 200 >$ and $< 300 >$ lamellar peaks are positioned along the q_z axis and the $< 010 > \pi - \pi$ peak is position along the q_x axis. The opposite can be seen in the electrosprayed samples in figure 4.3(b,d,f,h) where the $< 100 >$ lamellar peak is now positioned in the q_x axis and the $< 010 > \pi - \pi$ peak in the q_z axis. The $< 200 >$ and $< 300 >$ lamellar peaks are also present in the electrosprayed samples but are barely visible due to the low quantity of material of the electrosprayed samples leading to lower intensity of the diffracted x-rays. This shift in the position of the lamellar and $\pi - \pi$ peaks signals a shift in the orientation of the crystals in the films.

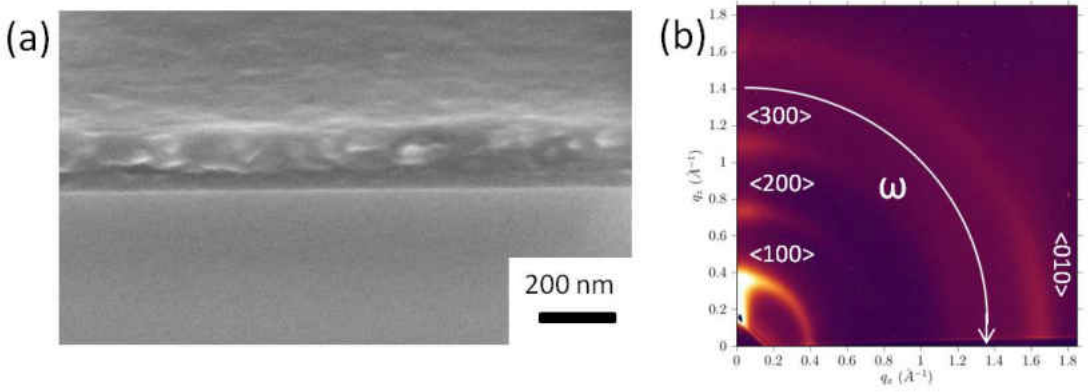

Figure 4.2: (a) SEM images of 1 wt % P3HT in Cholorobenze solution spin coated at 1000 rpm and (b) the corresponding GIXRD 2D intensity plot. The white line demonstrates the angles ω in which the polar profile cuts for figures 4.4 and 4.5 were taken.

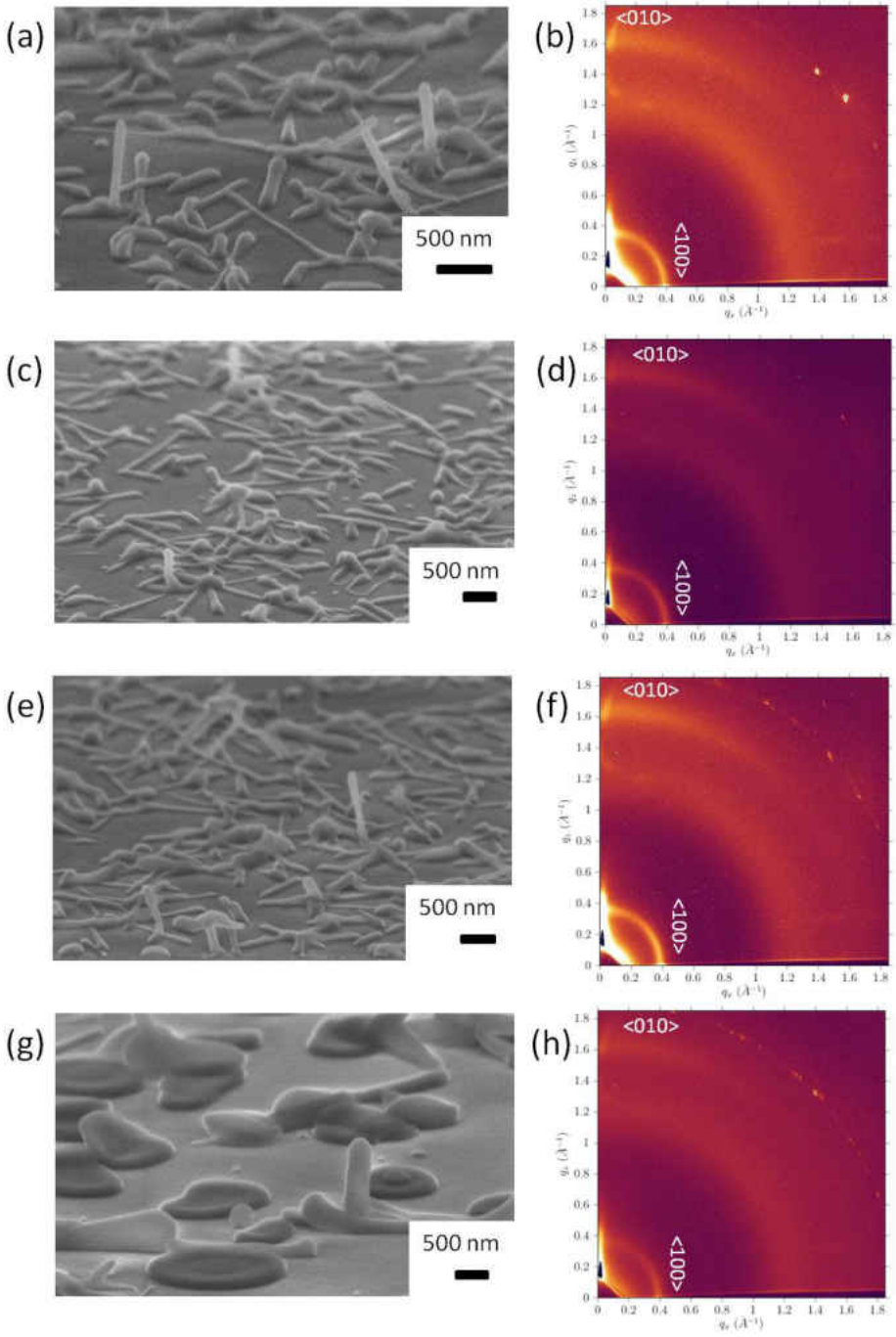

Figure 4.3: (a, c, e, g) SEM images of electrosprayed samples ES 1, ES 2, ES 3 and ES 4 respectively. (b, d, f, h) GIXRD 2D scattering intensity from samples ES 1, ES 2, ES 3 and ES 4.

Table 4.1: Name designation and process conditions for electrosprayed samples used for GIXRD analysis.

Sample	Flow rate	Electrical conductivity	Electric field
ES 1	60 µL/hr	~ 10^{-6} S/m	2 KV/mm
ES 2	60 µL/hr	~ 10^{-6} S/m	1 KV/mm
ES 3	60 µL/hr	~ 10^{-6} S/m	0.2 KV/mm
ES 4	100 µL/hr	~ 10^{-7} S/m	1 KV/mm

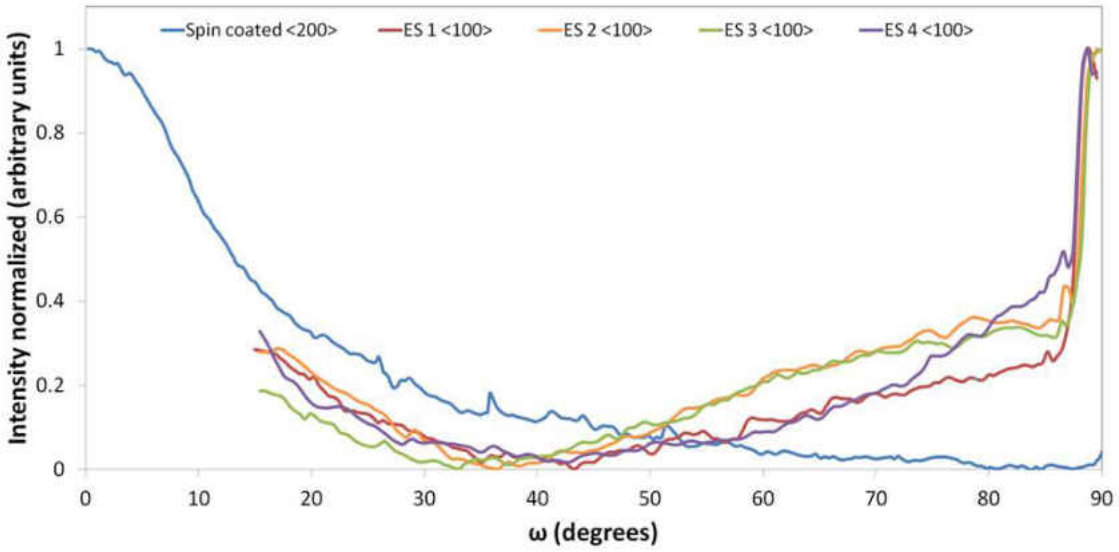

Figure 4.4: Polar profile cuts for all angles ω along radius pertaining to $< 100 >$ lamellar peak

To better illustrate the difference in the orientation of the crystals in spin coated and electrospray process, figures 4.4 and 4.5 show polar profile cuts along the lamellar $< 100 >$ peak at q=0.38 $\mathring{A}^{-1}$ and the $< 010 > \pi - \pi$ peak at q=1.64 $\mathring{A}^{-1}$ respectively. In figure 4.4, near $\omega = 0^o$, the spin coated control sample shows a higher intensity and decays as ω increases. The opposite is observed for the electrosprayed sample where the intensity in exponentially higher near $\omega = 90^o$.

Furthermore, in figure 4.5 the same effect is observed for the $< 010 > \pi - \pi$ peak. In this case, the spin coated samples has higher intensities near $\omega = 90^o$ and the electrosprayed samples near $\omega = 0^o$. Both these observations indicate a shift in alignment from edge-on in the spin coated samples to face-on in the electrosprayed samples in the majority of the crystals. There is not a distinct difference between the electrosprayed samples and can therefore be said that the electric field and the particle size does not significantly affect the orientation of the crystals in the presented electroprayed samples. Other studies have demonstrated similar results using grids to induce face-on orientation of the crystals [26] [2] [25].

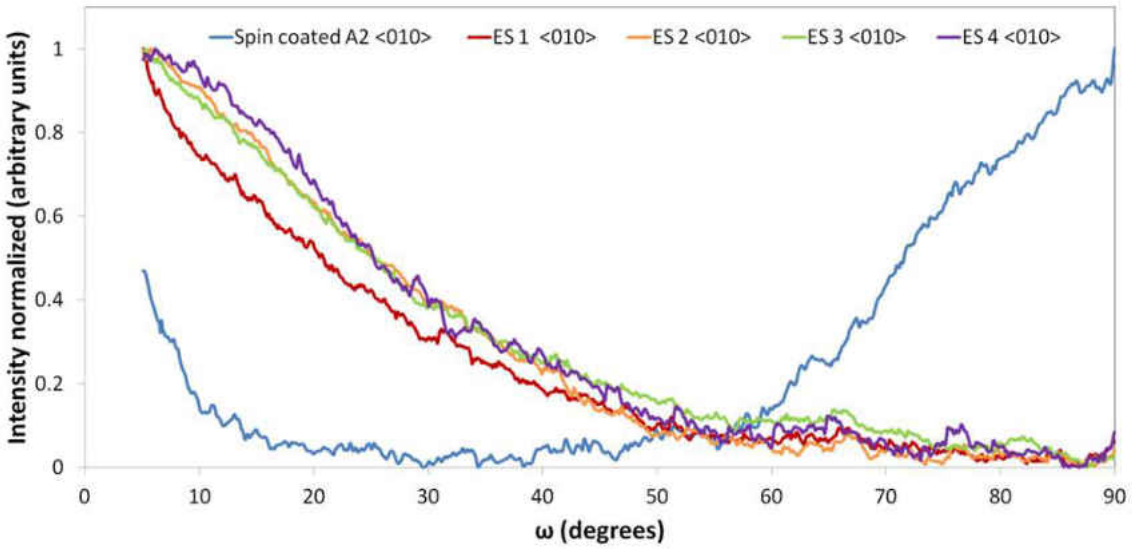

Figure 4.5: Polar profile cuts for all angles ω along radius pertaining to $< 010 > \pi - \pi$ peak

The size of the crystals in a particular direction can be estimated by using the Scherrer's equation (equation 4.3). Where τ is the mean size of the crystals, K is a dimensionless factor dependent of crystal shape, θ is the Bragg angle and $\Delta(2\theta)$ is the width of the peak at half the intensity.

$$\tau = \frac{K\lambda}{\Delta(2\theta)\cos\theta} \tag{4.3}$$

In figure 4.6, the profiles of the $< 100 >$ lamellar peaks can be seen for all the samples. The small circles in the plot are placed to represent where the peaks reached half of their particular intensity. Note, these profiles are different than the ones presented in figures 4.4 and 4.5 since these cut across as apposed to along the peaks. The values for K and λ in equation 4.3 are the same for all samples since all were tested at the same wavelength and the crystals are expected to have the same shape. Also, the value of the Bragg angle θ remains the same for all samples since all the profiles were taken for the $< 100 >$ lamellar peak. Then, the value of $\Delta(2\theta)$, which can be obtained from the profile cuts, becomes the only variable to find the mean crystal size τ. Visually, it is clear that the value of the $\Delta(2\theta)$ is nearly the same for all samples including the spin coated sample. The legend specifies the values of $\Delta(2\theta)$ which range from 0.65^o to 0.84^o. Although the values of $\Delta(2\theta)$ are not the same, the difference is not sufficient to draw the conclusion that the crystal size is different. The same is the case for the $< 010 > \pi - \pi$ peak presented in figure 4.7. It can then be concluded that the crystal size in the lamellar and $\pi - \pi$ directions are similar for the spin coated and the electrospray process. However, this conclusion does not exclude enhance crystal growth along the polymer backbone.

Ultraviolet-visible Spectroscopy

Ultraviolet and visible light absorbance spectrum profiles were obtained for the P3HT in solution, spin coated films and electrospray films. The absorbance spectrum is of interest due to the its relationship with the structure of the cystals. Two films of P3HT were prepared for the measurement, one film was spin coated and the other film was electrosprayed with the same parameters as those for the result presented in figure 3.6. As noted in the methods section, for this measurement the films were prepared on glass coated with fluorine doped tin oxide (FTO) and PEDOT:PSS. The absorbance profiles for P3HT disolved in cholorobenzene is presented in figure 4.8 and the processed

films are presented in figure 4.9.

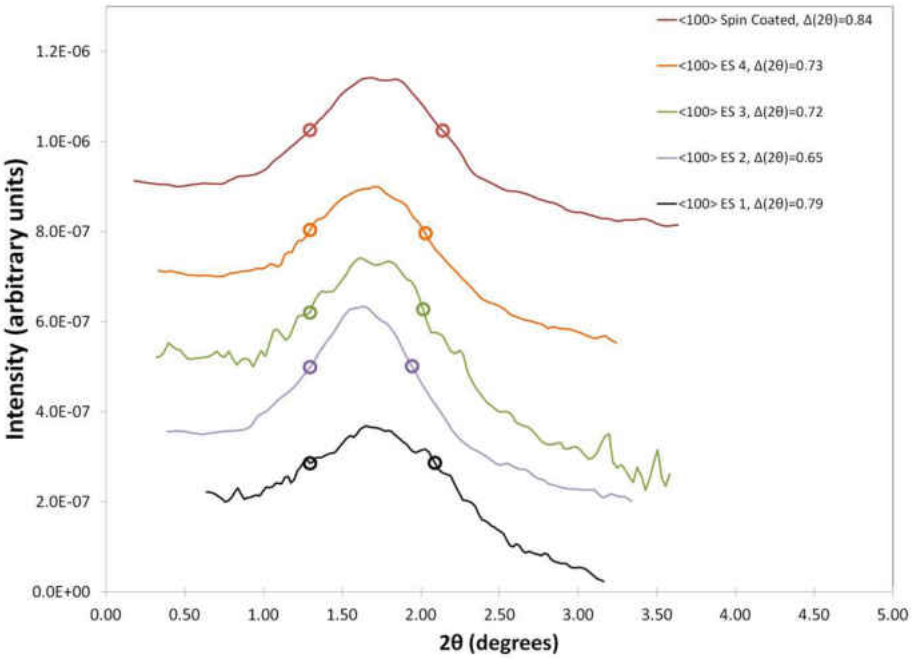

Figure 4.6: Intensity profiles lamellar $< 100 >$ peaks

During the solvent drying process as the films were prepared, the P3HT aggregates into crystals. This aggregation will cause the absorption spectrum to shift from absorbing shorter high energy waves peaking at 455 nm to absorbing longer low energy waves depending on the degree of crystallization [14]. This shift in the absorption spectrum towards larger wavelengths is commonly referred to as red-shift and the opposite is referred to as blue-shift. There are two observable differences in the absorbance profiles of the spin coated films and the electrosprayed films in figure 4.9. Most noticeable is a 22 nm red-shift of the electrospray sample as compared to the spin coated sample. As previously mentioned, the red-shift signals a higher degree of crystallization [14]. More specifically, the red-shift is interpreted as a higher degree of head to tail couplings along the polymer backbone and a higher degree of planar crystals[46]. The opposite case would be would

be a higher degree of head to head couplings along the polymer backbone leading to a blue-shift and less planar crystals.

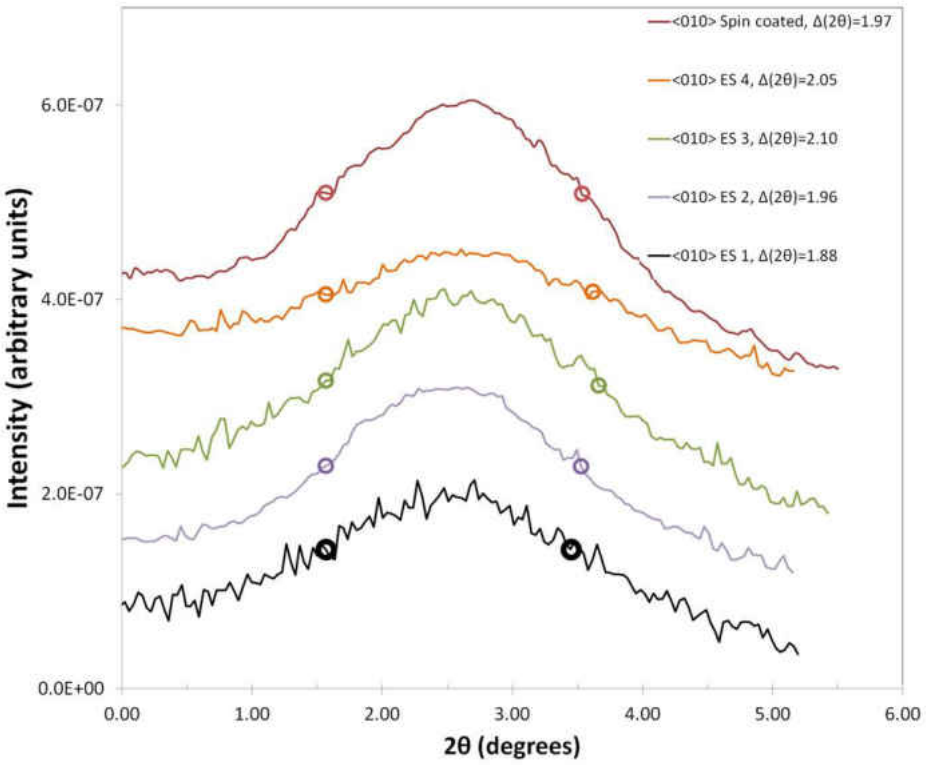

Figure 4.7: Intensity profiles $\pi - \pi < 010 >$ peaks

To further support this claim, the intensity ratio between the A_{00} and the A_{01}, $\frac{A_{00}}{A_{01}}$, is analyzed. The electrospray sample exhibits a $\frac{A_{00}}{A_{01}}$ ratio that is 31% larger than the spin coated sample. The $\frac{A_{00}}{A_{01}}$ is expressed by equation 4.4 where W is the exciton bandwidth and E_p is the main intramolecular vibration energy [40]. This equation dictates that an increase in $\frac{A_{00}}{A_{01}}$ leads to a decrease in the exciton bandwidth, W.

$$\frac{A_{00}}{A_{01}} = \frac{1 - 0.24W/E_p}{1 + 0.073W/E_p} \tag{4.4}$$

A decrease in the exciton bandwidth is interpreted as an increase in the conjugation length and

better intrachain order[11]. Hence, an increase in the $\frac{A_{00}}{A_{01}}$ ratio is the cause of longer conjugation length and more planar crystals. The aggregation of the P3HT is a competition of stacks along the $\pi - \pi$ direction and the head to tail couplings along the conjugation length [41]. Meaning that crystals with a larger conjugation length are expected to have less $\pi - \pi$ stacks. However, figure 4.7 demonstrates through Scherrer analysis that the length along the $\pi - \pi$ stacks remains roughly the same for electrosprayed samples and spin coated samples. As previously noted, studies have successfully demonstrated an increase in the conjugation length through thermally annealing samples [10][45][20][38]and processing in high boiling point solvents[11]. The charge mobility has been demonstrated to increase as the conjugation length increases [6]. The increase in the conjugation length for the mentioned studies is attributed to the longer processing times offered by thermal annealing and high boiling point solvents which allows the crystallites to grow. This is contrasting to the electrospray process where the solvent removal is fast and at room temperatures.

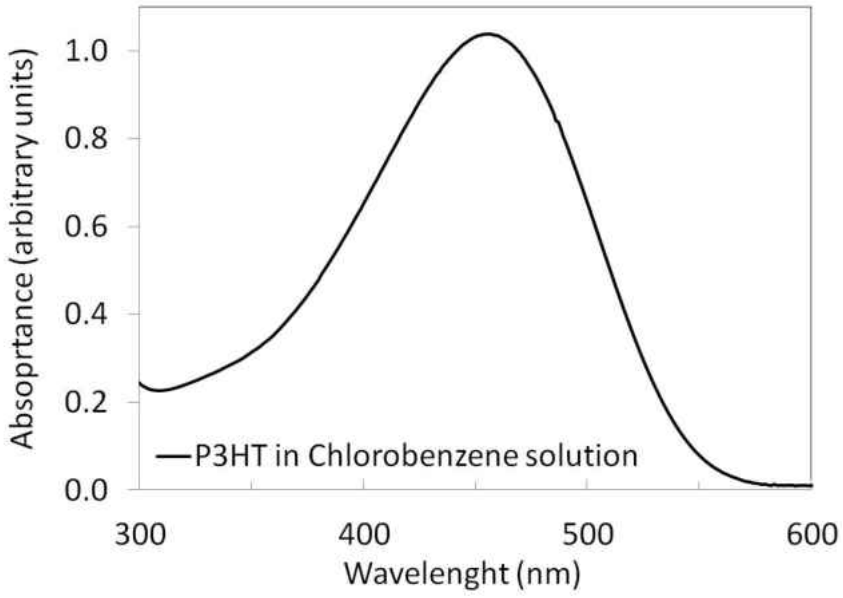

Figure 4.8: Absorbance profile of P3HT in solution of chlorobenze

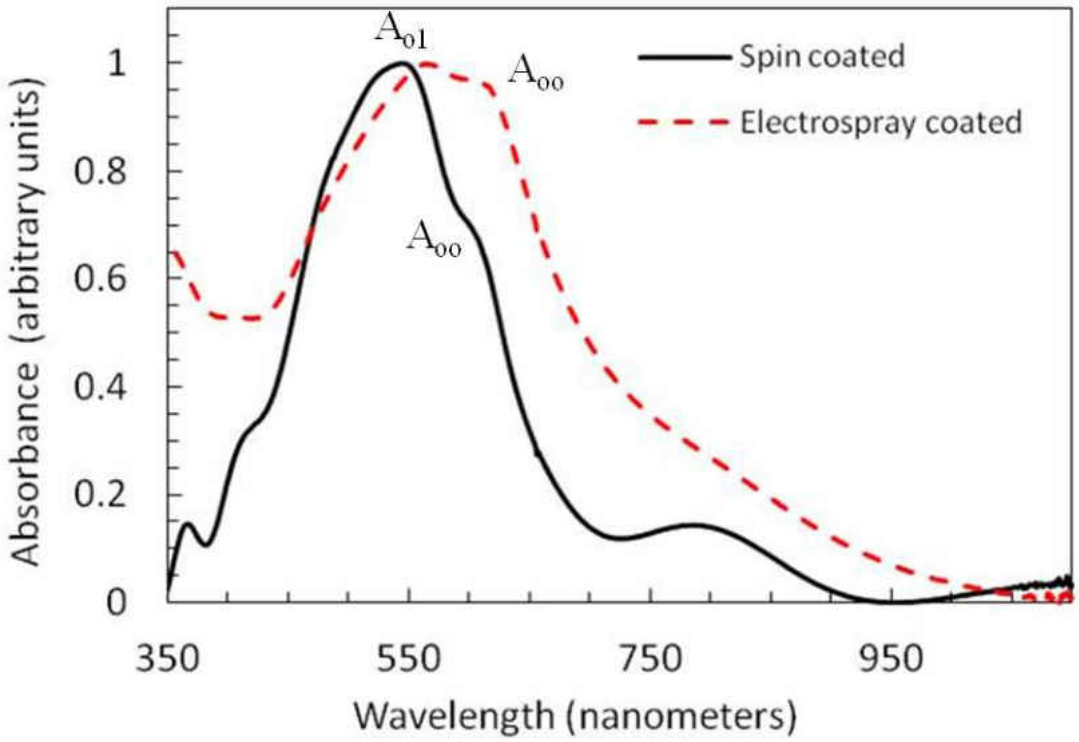

Figure 4.9: Absorbance profile of P3HT spin coated film and electrosprayed coated film

Conductive Atomic Force Microscopy

As mentioned previously in the Working distance section, it is important that the droplets make good contact with the substrate. To claim that the results presented in figure 3.6 is a structured film as oppose to a collection of particles, the electrical contact was characterized. Conductive Atomic Force Microscopy (CAFM) was utilized as the characterization tool as illustrated in figure 4.10. Note that the sample in the figure is illustrated as a P3HT/PCBM sample. The PCBM was introduced as a method to selectively transport current only through the P3HT. Since the work function of Platinum is higher than the HOMO value of the PCBM, an energy barrier prevents charge transport. To effectively conduct this measurement, it was necessary that the samples were

such that the P3HT pillars would protrude a continuous film of PCBM as illustrated in figure 4.10 as the P3HT pillars in red and the PCBM film in gold.

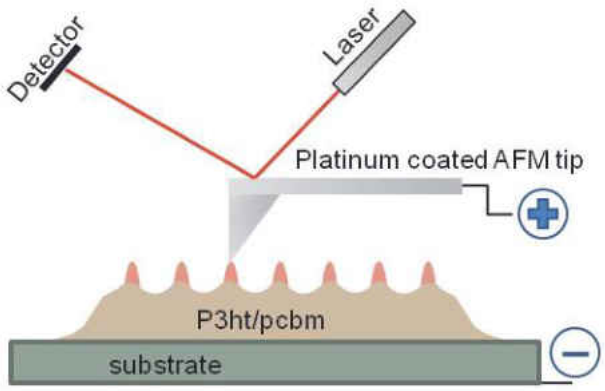

Figure 4.10: Conductive Atomic Force Microscopy setup with P3HT structured film semi saturated with PCBM

To fabricate the sample illustrated in figure 4.10, a dropcasting method was utilized to coat the PCBM after the samples were electrospray coated with P3HT. Dropcasting is a simple process where a drop of solution is deposite wet onto a substrate to make a film. Figure 4.11 illustrates a schematic and photograph of the dropcast setup utilized. The PCBM was processed as a solution in dichloromethane since it dissolves PCBM but not P3HT. The dichloromethane presented challenges due to its low boiling point (39.6^oC) which makes it a very volatile solvent. The fast evaporation of dichloromethane caused cooling of the substrate leading to condensation of the moisture in the air. The condensation on the substrate and the fast evaporation of the solvent resulted in very rough and discontinuous films. To increase the evaporation time, the dropcast process was perform on top a surfaced cooled to roughly 10^oC by use of a thermoelectric module. A large heat sink was necessary to be placed on the hot side of the thermoelectric to achieve a sufficient heat rate and maintain the cool side at low temperatures. A small clear plastic enclosure with a nitrogen feed was added to allow the process to take placed in a moisture free environment. The coating process

that minimizes moisture exposure is detailed in the following steps.

- Place sample on top of the cool side of the thermoelectric module, seal with clear plastic enclosure and open nitrogen feed.
- Allow 5 minutes for the nitrogen to remove all the moisture from the enclosed space, turn on the thermoelectric module and wait for the power supply to reach a steady desired voltage.
- Close the nitrogen feed, quickly insert the needle and deposit the solution on top of the sample.
- Wait for the solvent to dry.
- When the solvent is observably dried, open the nitrogen feed for roughly 1 minute.
- Power off the themoelectric module and wait 2 minutes to allow sample to reach room temperature.
- Open the enclosure and remove the sample.

Another factor to take into consideration is the leveling of the setup. If the sample well leveled, the liquid will accumulate in one side.

The samples resulting the the process described above are presented in figures 4.12 and 4.13 at different magnifications. The quality of the samples in the film continuity and protrusion of the P3HT pillars depends mostly on the density of the P3HT deposition and the concentration of the PCBM solution being deposited. A P3HT coating density that was low would typically result in samples that had discontinuities in the PCBM coating. A low concentration of PCBM in the dropcast solution would also result in discontinuities. However, a PCBM concentration that was too high would result in a smooth thick film of PCBM completely enclosing the P3HT pillars. It

was determined that a concentration of 0.5 wt % yielded the best results as presented in figures 4.12 and 4.13. Near the top of figure 4.12(a) the noted discontinuities in the film can be observed. However, the sample presented in figure 4.13 appears to be fully continuous. The difference in the two samples is the density of P3HT features with the sample in figure 4.13 having twice the density of P3HT. Note that the sample in figure 4.12 would still be useful for the CAFM measurement but a location continuous PCBM would first need to be located.

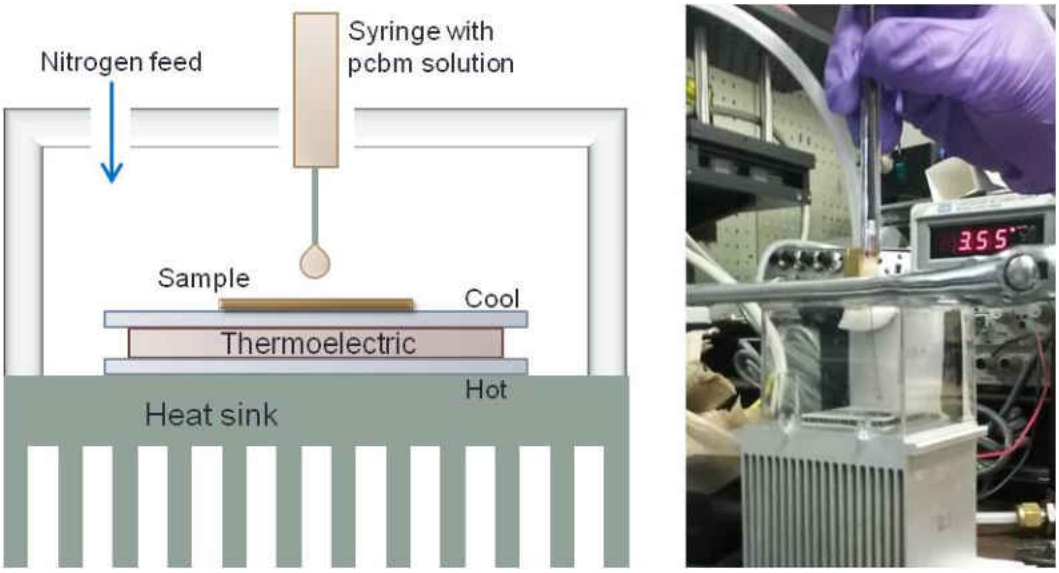

Figure 4.11: Dropcast setup for coating of PCBM in dichloromethane solution. Schematic on the left and photograph in the right.

As mentioned, the importance of fabricating the P3HT samples semi saturated in PCBM was to selectively record a electrical current response through the P3HT to confirm its contact with the substrate. The topography and the electrical current of the sample presented in figure 4.13 was characterized simultaneously using the CAFM. The height and current results presented in figure 4.14 shows the similarity of the both sets of data for the same spot in the sample. It can be observed that both the height and the current have the same peaks present in the same positions. Also, the electrical current is only conducted through the peaks meaning that the peaks are the only places

where P3HT is expose. Most importantly, the presence of an electrical signal through the P3HT confirms that the pillars have good contact with the substrate. Hence, this result confirms that the samples presented can be considered structured films.

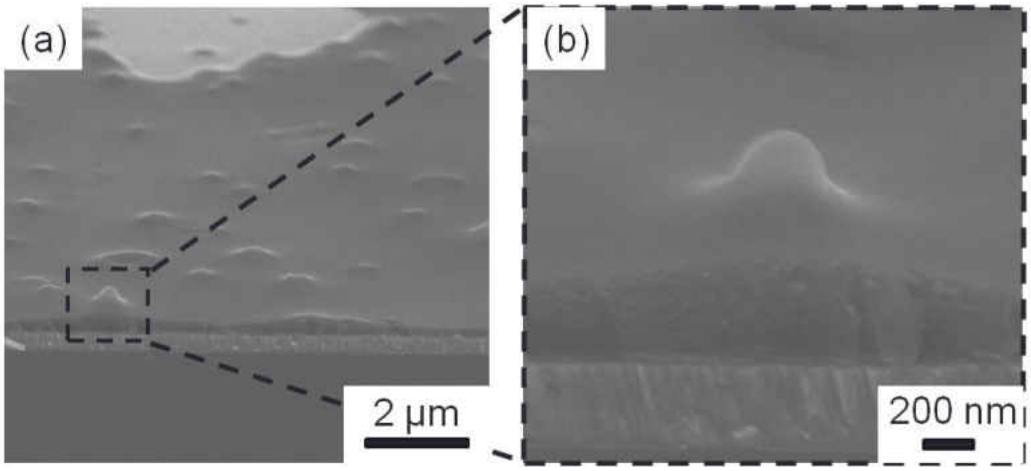

Figure 4.12: SEM image at (a) 20 KX and (b)100 KX magnification and 70^o perspective

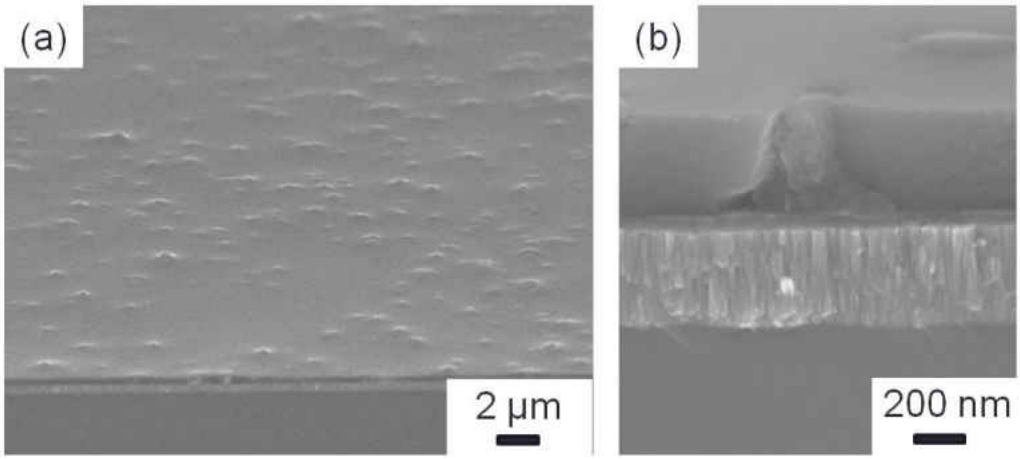

Figure 4.13: SEM image at (a) 5 KX and (b)100 KX magnification and 70^o perspective

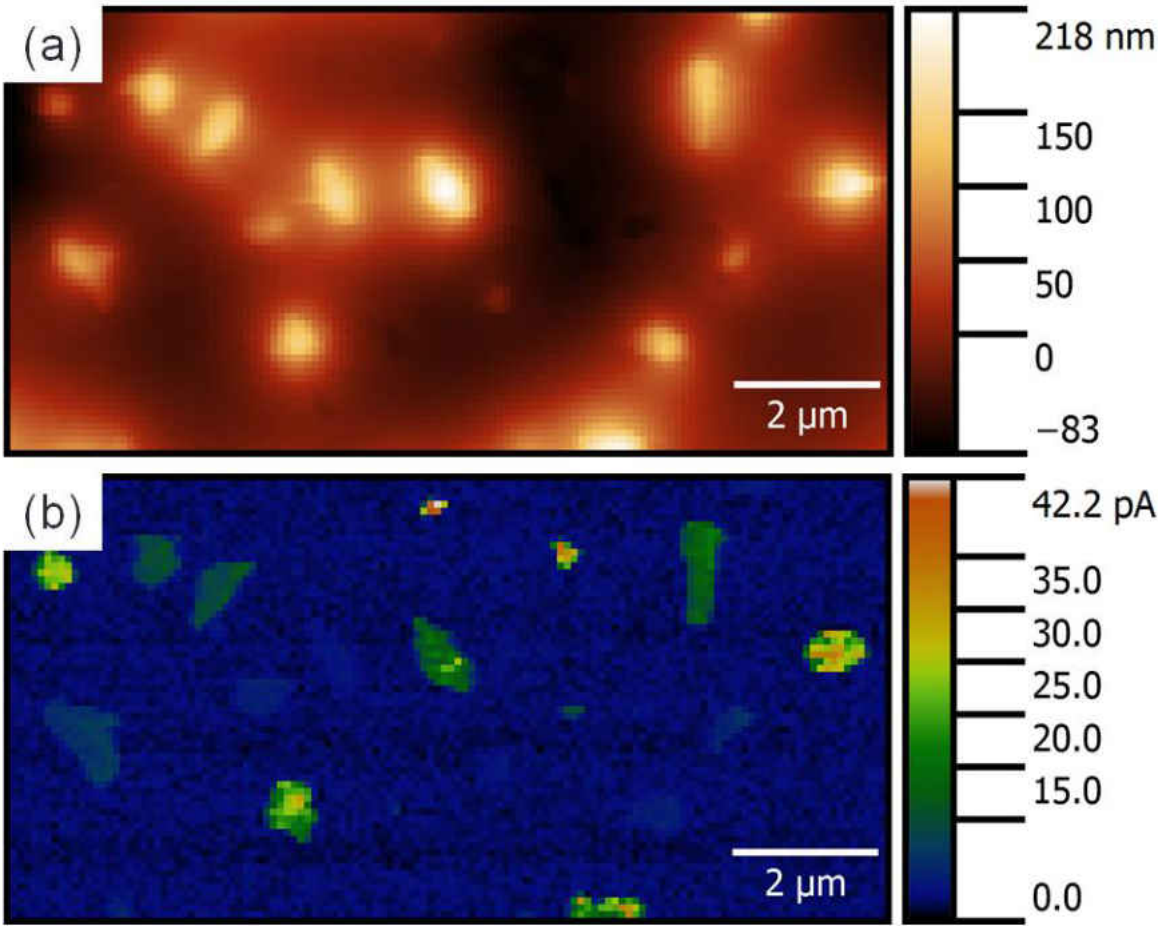

Figure 4.14: (a) Height and (b) electrical current CAFM data plots for sample presented in figure 4.13. The voltage drop was set to 5 volts during the measurements.

CHAPTER 5: CONCLUSION

In this study the ability of electrospray to process P3HT solutions into films of different morphologies has been demonstrated. Of most importance are the films with the high aspect ratio features presented in figure 3.6. Also, the nozzle design using the drillbit can be considered a simple solution to a significant problem with the electrospray stability. The simplicity of the solution and the ready availability of the components make it easy to replicate and will hopefully help future similar studies. In addition to the results presented in the process development, the crystallinity and the orientation of the P3HT crystals within the amorphous matrix of P3HT was demonstrated to be affected by the electrospray process. These effects of the electrospray on the crystals are attributed to the large degree of surface area of the droplets present during the spray process. Other studies have demonstrated an enhancing effect of the surface on the crystallinity and orientation of polyimide [21] and P3HT [29]. Although, the observations of the mentioned studies were on a smooth silicon interface. Of most relevance is the demonstratio of a new effect electrospray has on the crystallinity.

Future research is recommended for a new generation of conjugated polymers. Figure 5.1 shows the results of electrospray deposition of a conjugated polymer known as PBDTT-FTTE. In the application of organic solar cells, this material has demonstrated a power efficiency of 10.3% [1] in comparison to a 5.6% reported for P3HT [13]. The preliminary results in figure 5.1 show structures that could enhance organic solar cells by approaching the ideal ordered bulk heterojunction structure [13]. It is recommended that the crystallinity be characterized in the same manner presented in this study to determine if the results are applicable to multiple materials. Also, solar cells could be fabricated and tested to observe the end results of the electrospray process on a device.

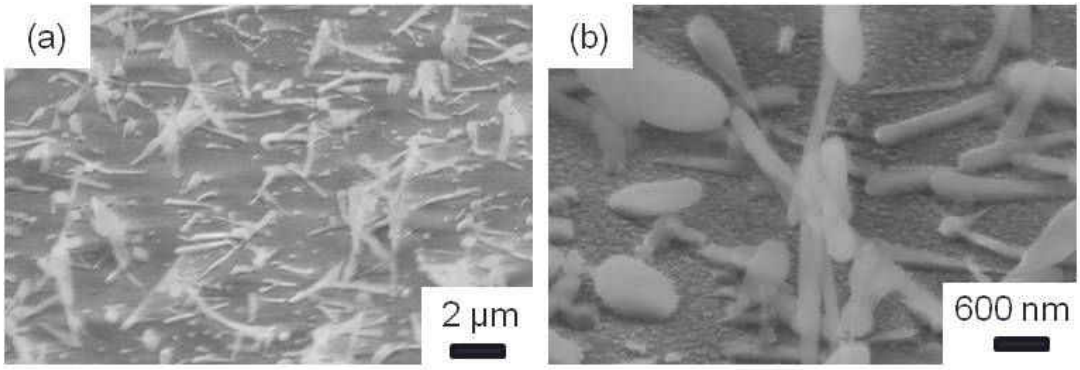

Figure 5.1: (a) SEM image of electrospray of 1 wt % of PBDTT-FTTE conjugated polymer solution. (b) Higher magnification.

LIST OF REFERENCES

[1] *Solarmer Organic Electronics*.

[2] Jonathan E. Allen, Kevin G. Yager, Htay Hlaing, Chang-Yong Nam, Benjamin M. Ocko, and Charles T. Black. Enhanced charge collection in confined bulk heterojunction organic solar cells. *Applied Physics Letters*, 99(16):–, 2011.

[3] Begona Almeria, Weiwei Deng, Tarek M. Fahmy, and Alessandro Gomez. Controlling the morphology of electrospray-generated plga microparticles for drug delivery. *Journal of Colloid and Interface Science*, 343(1):125 – 133, 2010.

[4] Begona Almeria and Alessandro Gomez. Electrospray synthesis of monodisperse polymer particles in a broad (60 nm2m) diameter range: guiding principles and formulation recipes. *Journal of Colloid and Interface Science*, 417(0):121 – 130, 2014.

[5] K. Altmann, R.-D. Schulze, and J. Friedrich. Polymer deposition morphology by electrospray deposition - modifications through distance variation. *Thin Solid Films*, 564(0):269 – 276, 2014.

[6] Jui-Fen Chang, Baoquan Sun, Dag W. Breiby, and Martin M. Nielsen. Enhanced mobility of poly(3-hexylthiophene) transistor by spin-coating from high-boiling-point solvents. *American Chemical Society*, 16(23):4772 – 4776, 2004.

[7] Shun-Chi Chang, Jie Liu, Jayesh Bharathan, Yang Yang, Jun Onohara, and Junji Kido. Multicolor organic light-emitting diodes processed by hybrid inkjet printing. *Advanced Materials*, 11(9):734–737, 1999.

[8] Da-Ren Chen and David Y. H. Pui. Experimental investigation of scaling laws for electrospraying: Dielectric constant effect. *Aerosol Science and Technology*, 27(3):367–380, 1997.

[9] Da-Ren Chen, David Y.H. Pui, and Stanley L. Kaufman. Electrospraying of conducting liquids for monodisperse aerosol generation in the 4 nm to 1.8 m diameter range. *Journal of Aerosol Science*, 26(6):963 – 977, 1995.

[10] D Chirvase, J Parisi, J C Hummelen, and V Dyakonov. Influence of nanomorphology on the photovoltaic action of polymerfullerene composites. *Nanotechnology*, 15(9):1317, 2004.

[11] Jenny Clark, Jui-Fen Chang, Frank C. Spano, Richard H. Friend, and Carlos Silva. Determining exciton bandwidth and film microstructure in polythiophene films using linear absorption spectroscopy. *Applied Physics Letters*, 94(16):–, 2009.

[12] Michel Cloupeau and Bernard Prunet-Foch. Electrohydrodynamic spraying functioning modes: a critical review. *Journal of Aerosol Science*, 25(6):1021 – 1036, 1994.

[13] Kevin M Coakley and Michael D McGehee. Conjugated polymer photovoltaic cells. *Chemistry of materials*, 16(23):4533–4542, 2004.

[14] Edward J. W. Crossland, Khosrow Rahimi, Gnter Reiter, Ullrich Steiner, and Sabine Ludwigs. Systematic control of nucleation density in poly(3-hexylthiophene) thin films. *Advanced Functional Materials*, 21(3):518–524, 2011.

[15] J. Fernndez De La Mora and I. G. Loscertales. The current emitted by highly conducting taylor cones. *Journal of Fluid Mechanics*, 260:155–184, 2 1994.

[16] Weiwei Deng and Alessandro Gomez. Influence of space charge on the scale-up of multiplexed electrosprays. *Journal of Aerosol Science*, 38(10):1062–1078, 2007.

[17] Weiwei Deng and Alessandro Gomez. The role of electric charge in microdroplets impacting on conducting surfaces. *Physics of Fluids*, 22(5):–, 2010.

[18] Weiwei Deng, James F. Klemic, Xiaohui Li, Mark A. Reed, and Alessandro Gomez. Increase of electrospray throughput using multiplexed microfabricated sources for the scalable generation of monodisperse droplets. *Journal of Aerosol Science*, 37(6):696 – 714, 2006.

[19] Weiwei Deng, C. Mike Waits, Brian Morgan, and Alessandro Gomez. Compact multiplexing of monodisperse electrosprays. *Journal of Aerosol Science*, 40(10):907 – 918, 2009.

[20] Tobias Erb, Uladzimir Zhokhavets, Harald Hoppe, Gerhard Gobsch, Maher Al-Ibrahim, and Oliver Ambacher. Absorption and crystallinity of poly(3-hexylthiophene)/fullerene blends in dependence on annealing temperature. *Thin Solid Films*, 511512(0):483 – 485, 2006. EMSR 2005 - Proceedings of Symposium F on Thin Film and Nanostructured Materials for Photovoltaics EMRS 2005- Symposium F EMSR 2005 - Proceedings of Symposium F on Thin Film and Nanostructured Materials for Photovoltaics.

[21] BJ Factor, TP Russell, and MF Toney. Surface-induced ordering of an aromatic polyimide. *Physical review letters*, 66(9):1181, 1991.

[22] A.M. Ganan-Calvo, J. Davila, and A. Barrero. Current and droplet size in the electrospraying of liquids. scaling laws. *Journal of Aerosol Science*, 28(2):249 – 275, 1997.

[23] Alessandro Gomez and Keqi Tang. Charge and fission of droplets in electrostatic sprays. *Physics of Fluids*, 6(1), 1994.

[24] R.P.A. Hartman, D.J. Brunner, D.M.A. Camelot, J.C.M. Marijnissen, and B. Scarlett. Jet break-up in electrohydrodynamic atomization in the cone-jet mode. *Journal of Aerosol Science*, 31(1):65 – 95, 2000.

[25] Htay Hlaing, Xinhui Lu, Tommy Hofmann, Kevin G. Yager, Charles T. Black, and Benjamin M. Ocko. Nanoimprint-induced molecular orientation in semiconducting polymer nanostructures. *ACS Nano*, 5(9):7532–7538, 2011. PMID: 21838293.

[26] Danvers E. Johnston, Kevin G. Yager, Htay Hlaing, Xinhui Lu, Benjamin M. Ocko, and Charles T. Black. Nanostructured surfaces frustrate polymer semiconductor molecular orientation. *ACS Nano*, 8(1):243–249, 2014. PMID: 24341785.

[27] Sang-Yoon Kim, Jaehong Park, and Jungho Hwang. Design and evaluation of single nozzle with a non-conductive tip for reducing applied voltage and pattern width in electrohydrodynamic jet printing (ehdp). *Journal of Micromechanics and Microengineering*, 2010.

[28] R Joseph Kline, Michael D McGehee, Ekaterina N Kadnikova, Jinsong Liu, Jean MJ Fréchet, and Michael F Toney. Dependence of regioregular poly (3-hexylthiophene) film morphology and field-effect mobility on molecular weight. *Macromolecules*, 38(8):3312–3319, 2005.

[29] R Joseph Kline, Michael D McGehee, and Michael F Toney. Highly oriented crystals at the buried interface in polythiophene thin-film transistors. *Nature Materials*, 5(3):222–228, 2006.

[30] Marion Sausse Lhernould and Pierre Lambert. Compact polymer multi-nozzles electrospray device with integrated microfluidic feeding system. *Journal of Electrostatics*, 69(4):313 – 319, 2011.

[31] J.L. Li. Formation and stabilization of an ehd jet from a nozzle with an inserted non-conductive fibre. *Journal of Aerosol Science*, 36(3):373 – 386, 2005.

[32] Brandon Lojewski, Weiwei Yang, Hongxu Duan, Chengying Xu, and Weiwei Deng. Design, fabrication, and characterization of linear multiplexed electrospray atomizers micromachined from metal and polymers. *Aerosol Science and Technology*, 47(2):146–152, 2013.

[33] Fanzheng Meng, Yi Jiang, Zhihui Sun, Yizi Yin, and Yanyan Li. Electrohydrodynamic liquid atomization of biodegradable polymer microparticles: Effect of electrohydrodynamic liquid

atomization variables on microparticles. *Journal of Applied Polymer Science*, 113(1):526–534, 2009.

[34] Lord Rayleigh. On the capillary phenomena of jets. In *Proc. R. Soc. London*, volume 29, pages 71–97, 1879.

[35] Lord Rayleigh. On the equilibrium of liquid conducting masses charged with electricity. *Philosophical Magazine Series 5*, 14(87):184–186, 1882.

[36] Chang Seoul and Nam-Hee Kim. Polymer light-emitting diodes based on poly(3-hexyl thiophene). *Fibers and Polymers*, 1(1):25–31, 2000.

[37] Sean E Shaheen, Rachel Radspinner, Nasser Peyghambarian, and Ghassan E Jabbour. Fabrication of bulk heterojunction plastic solar cells by screen printing. *Applied Physics Letters*, 79(18):2996–2998, 2001.

[38] Henning Sirringhaus, PJ Brown, RH Friend, Martin Meedom Nielsen, Klaas Bechgaard, BMW Langeveld-Voss, AJH Spiering, Rene AJ Janssen, EW Meijer, P Herwig, et al. Two-dimensional charge transport in self-organized, high-mobility conjugated polymers. *Nature*, 401(6754):685–688, 1999.

[39] Henning Sirringhaus, Nir Tessler, and Richard H. Friend. Integrated optoelectronic devices based on conjugated polymers. *Science*, 280(5370):1741–1744, 1998.

[40] Frank C. Spano. Modeling disorder in polymer aggregates: The optical spectroscopy of regioregular poly(3-hexylthiophene) thin films. *The Journal of Chemical Physics*, 122(23):–, 2005.

[41] Frank C. Spano and Carlos Silva. H- and j-aggregate behavior in polymeric semiconductors. *Annual Review of Physical Chemistry*, 65(1):477–500, 2014. PMID: 24423378.

[42] Marshall L. Sweet, Dmitry Pestov, Gary C. Tepper, and James T. McLeskey Jr. Electrospray aerosol deposition of water soluble polymer thin films. *Applied Surface Science*, 289(0):150 – 154, 2014.

[43] Keqi Tang and Alessandro Gomez. On the structure of an electrostatic spray of monodisperse droplets. *Physics of Fluids*, 6(7), 1994.

[44] Stephen R Turns et al. *An introduction to combustion 2nd edition*. McGraw-hill Boston, 2006.

[45] Svetlana S. van Bavel, Maik Brenklau, Gijsbertus de With, Harald Hoppe, and Joachim Loos. P3ht/pcbm bulk heterojunction solar cells: Impact of blend composition and 3d morphology on device performance. *Advanced Functional Materials*, 20(9):1458–1463, 2010.

[46] Bai Xu and Steven Holdcroft. Molecular control of luminescence from poly(3-hexylthiphenes. *Macromolecules*, 26(17):4457–4460, 2011.

[47] Weiwei Yang, Brandon Lojewski, Yan Wei, and Weiwei Deng. Interactions and deposition patterns of multiplexed electrosprays. *Journal of Aerosol Science*, 46(0):20 – 33, 2012.

[48] Gang Yu, Jun Gao, Jan C Hummelen, Fred Wudl, and Alan J Heeger. Polymer photovoltaic cells: enhanced efficiencies via a network of internal donor-acceptor heterojunctions. *Science-AAAS-Weekly Paper Edition*, 270(5243):1789–1790, 1995.

[49] John Zeleny. The electrical discharge from liquid points, and a hydrostatic method of measuring the electric intensity at their surfaces. *Phys. Rev.*, 3:69–91, Feb 1914.

[50] John Zeleny. Instability of electrified liquid surfaces. *Phys. Rev.*, 10:1–6, Jul 1917.

[51] Xin-Yan Zhao, Xizu Wang, Siew Lay Lim, Dongchen Qi, Rui Wang, ZhiQiang Gao, BaoXiu Mi, Zhi-Kuan Chen, Wei Huang, and Weiwei Deng. Enhancement of the performance of

organic solar cells by electrospray deposition with optimal solvent system. *Solar Energy Materials and Solar Cells*, 121(0):119 – 125, 2014.